

Necessary conditions for a maximum likelihood estimate to become asymptotically unbiased and attain the Cramer–Rao lower bound. II. Range and depth localization of a sound source in an ocean waveguide

Aaron Thode, Michele Zanolin, Eran Naftali, Ian Ingram, Purnima Ratilal,
and Nicholas C. Makris

Ocean Engineering Department, Massachusetts Institute of Technology, Cambridge, Massachusetts 02139

(Received 17 October 2000; revised 24 September 2001; accepted 29 May 2002)

Analytic expressions for the first order bias and second order covariance of a maximum-likelihood estimate (MLE) are applied to the problem of localizing an acoustic source in range and depth in a shallow water waveguide with a vertical hydrophone array. These expressions are then used to determine *necessary* conditions on sample size, or equivalently signal-to-noise ratio (SNR), for the localization MLE to become asymptotically unbiased and attain minimum variance as expressed by the Cramer–Rao lower bound (CRLB). These analytic expressions can be applied in a similar fashion to any ocean-acoustic inverse problem involving random data. Both deterministic and completely randomized signals embedded in independent and additive waveguide noise are investigated. As the energy ratio of received signal to additive noise (SANR) descends to the lower operational range of a typical passive localization system, source range and depth estimates exhibit significant biases and have variances that can exceed the CRLB by orders of magnitude. The spatial structure of the bias suggests that acoustic range and depth estimates tend to converge around particular range and depth cells for moderate SANR values. © 2002 Acoustical Society of America. [DOI: 10.1121/1.1496765]

PACS numbers: 43.30.Wi, 43.60.Rw, 43.60.Gk [DLB]

I. INTRODUCTION

In recent years, many acoustic techniques have been developed to probe the marine environment. These techniques typically require the nonlinear inversion of acoustic field data measured by a hydrophone array.^{1–3} The data, however, are often randomized by the addition of natural ambient noise, or by fluctuations in the acoustic source, waveguide refractive index, and waveguide boundaries. Since the nonlinear inversion of random data often yields estimates with biases and mean-square errors that are difficult to quantify, it has become popular to simply neglect these potential biases and to compute limiting bounds on the mean-square error, since the bounds are usually much easier to obtain than the actual mean-square errors. The most widely used limiting bound is the Cramer–Rao lower bound (CRLB),⁴ which describes the minimum possible variance of any unbiased estimator, and has been introduced in the ocean acoustic source localization literature via Refs. 5 and 6, for example. Other bounds, however, also exist in the literature,^{7–11} that are not directly relevant to the present work.

The purpose of the present paper is not to apply a new general bound, but to demonstrate how the asymptotic properties of the maximum likelihood estimate (MLE) described in a companion paper¹² can be used to better understand the statistical errors and biases that occur in a typical ocean acoustic inverse problem. The MLE has a straightforward implementation. It is obtained by maximizing the likelihood function with respect to the parameter vector to be estimated,

where the likelihood function is the conditional probability density of the data, given the unknown parameter vector, evaluated at the measured data values. The MLE is widely used in statistics, because if an estimator becomes asymptotically unbiased and attains the CRLB for large sample sizes or high signal-to-noise ratio (SNR), it is guaranteed to be the MLE.⁴ It follows that an analysis of the conditions necessary for a MLE to become unbiased and attain minimum-variance, and thus optimal performance, will also reveal the conditions necessary for *any* nonlinear estimate to asymptotically achieve optimal performance.

In ocean-acoustic inverse problems, the likelihood function can be maximized by an exhaustive or directed search via forward modeling with numerical wave propagation or scattering algorithms. While the linear least squares estimator is also a widely used inversion scheme in acoustics and geophysics,¹³ it is only identical to the MLE when the data and parameter vectors are linearly related, and when the data are uncorrelated, follow a multivariate Gaussian distribution, and share the same variance.¹⁴ Since these conditions are often not satisfied in practice, the linear least squares estimator is often suboptimal even in the asymptotic regime of high SNR, making the MLE a preferable choice.

The present application concerns the classic ocean-acoustic inverse problem of localizing a source in range and depth in a shallow water waveguide, using data received on a vertical hydrophone array,³ also known as the “matched-field

processing” (MFP) source localization problem.^{2,16} [There are differences between some standard matched field processors and the MLE that have sometimes gone unnoticed in the MFP literature. For example, the “minimum-variance distortionless response (MVDR) processor,” which is presented as a MLE in Refs. 3 and 5, is neither a minimum-variance estimator nor the MLE for range and depth localization in a waveguide, as discussed by Sullivan and Middleton.¹⁵ The MVDR processor is a MLE, however, for the particular problem of estimating the complex amplitude of a plane wave arriving from a *known* direction, in independent additive Gaussian noise.] Here the theory presented in the companion paper¹² is used to set conditions on the sample size and SNR *necessary* for the MLE to become asymptotically unbiased and attain the CRLB in MFP source localization. These conditions can also be used in experimental design and analyses to ensure that statistical biases and errors are maintained within tolerable limits set by the given scientific or engineering objective. The approach follows that given in Ref. 12 and is based on the fact that the MLE can be expanded as an asymptotic series in inverse orders of sample size¹⁷ or equivalently an appropriately defined SNR. From this series, analytic expressions for the first order bias and second order error correlation of a general MLE can be found in terms of the joint moments of parameter derivatives of the log-likelihood function.¹² Since the first order error correlation is the CRLB, which is only valid for unbiased estimates, the second order error correlation can provide a better estimate of the MLE mean-square error that is applicable at relatively low SNR, even when the MLE is biased to first order. Necessary conditions for asymptotic optimality of the MLE are then obtained by demonstrating when the first order bias becomes negligible compared to the true value of the parameter, and when the second order error correlation becomes negligible compared to the CRLB.¹²

In this paper the localization performance of the MLE for both deterministic and randomized monopole signals embedded in independent, additive waveguide noise is analyzed. As the energy ratio of received signal to additive noise (SANR) descends to the lower operational range of a typical passive localization system, the range and depth MLE demonstrates significant bias and has a mean-square error that exceeds the CRLB by orders of magnitude.

II. ASYMPTOTIC STATISTICS

A. Preliminary definitions

Following the theory and notation adopted in paper I,¹² let the random data vector \mathbf{X} , given m -dimensional parameter vector $\boldsymbol{\theta}$, obey the conditional probability density function (PDF) $p(\mathbf{X}; \boldsymbol{\theta})$. The log-likelihood function $l(\boldsymbol{\theta})$ is then defined as $l(\boldsymbol{\theta}) = \ln(p(\mathbf{X}; \boldsymbol{\theta}))$, when evaluated at the measured values of \mathbf{X} . The first-order parameter derivative of the log-likelihood function is then defined as $l_r = \partial l(\boldsymbol{\theta}) / \partial \theta^r$, where θ^r is the r th component of $\boldsymbol{\theta}$. Moments of the log-likelihood

derivatives are defined by $v_R \equiv E[l_R]$, where R is an arbitrary set of indices. If $R_1 = r_{11} \dots r_{1n_1}, \dots, R_m = r_{m1} \dots r_{mn_m}$ are sets of coordinate indices in the parameter space, joint moments of the log-likelihood derivatives can be defined by $v_{R_1, R_2, \dots, R_M} \equiv E[l_{R_1} l_{R_2} \dots l_{R_M}]$, where, for example, $v_{s, tu} = E[l_s l_{tu}]$ and $v_{a, b, c, de} = E[l_a l_b l_c l_{de}]$.

The expected information, known as the Fisher information, is defined as $i_{rs} = E[l_r l_s]$, for arbitrary indices r, s .⁴ Lifting the indices produces quantities that are defined as¹⁷

$$v^{R_1, R_2, \dots, R_M} = i^{r_1 s_1} i^{r_2 s_2} \dots i^{r_{n_1} s_{n_1}} i^{r_{21} s_{21}} i^{r_{22} s_{22}} \dots i^{r_{mn_m} s_{mn_m}} \times v_{s_1 s_2 \dots s_{n_1} s_{21} s_{22} \dots s_{mn_m}}, \quad (1)$$

where $i^{rs} = [\mathbf{i}^{-1}]_{rs}$. Here, as elsewhere, the Einstein summation convention is used, so that whenever an index appears as both a superscript and subscript in a term, summation over that index is implied. The Fisher information matrix, \mathbf{i} , has an inverse \mathbf{i}^{-1} , known as the Cramer–Rao lower bound (CRLB),^{4,14,18} which is a lower bound on the minimum variance an unbiased estimator can attain.

B. General asymptotic expansions for the bias and covariance of the MLE

With the notation presented in Sec. II A, the first-order bias of the MLE can be written as^{12,17}

$$b(\hat{\boldsymbol{\theta}}^r) = E[(\hat{\boldsymbol{\theta}} - \boldsymbol{\theta})^r] = \underbrace{\frac{1}{2} i^{ra} i^{bc} (v_{abc} + 2v_{a, bc})}_{O_p(n^{-1})} + O_p(n^{-2}) + \dots, \quad (2)$$

where the symbol $O_p(n^{-m})$ denotes a polynomial of exactly order n^{-m} , where n is the sample size. It is noteworthy that third derivatives of the log-likelihood function may be necessary to compute the first-order bias.

A *necessary* condition for the MLE to become asymptotically unbiased is for the first-order terms in Eq. (2) to become much smaller than the true value of the parameter θ^r . Equation (2) may then be used to determine the minimum sample size n necessary for the MLE to become effectively unbiased.

An expression for the asymptotic covariance of the MLE has been derived by Naftali and Makris in paper I,¹² who obtained the first two asymptotic orders of the MLE covariance as

$$\begin{aligned}
\text{cov}(\hat{\theta}^r, \hat{\theta}^a) &= E[(\hat{\theta}^r - E[\hat{\theta}^r])(\hat{\theta}^a - E[\hat{\theta}^a])] \\
&= \underbrace{\left[i^{ra} \right]}_{O_p(n^{-1})} + \underbrace{\left[2i^{mb}i^{nc}v_{lmn}(r^{rs}i^{la} + i^{as}i^{lr})v_{s,b,c}(n^1) + \frac{1}{2}i^{cd}i^{ef}(i^{rs}i^{ab} + i^{as}i^{rb})v_{bce,d,f,s}(n^2) \right]}_{O_p(n^{-2})} \\
&\quad + \underbrace{i^{tu}(i^{rs}i^{ab}i^{cd} + i^{rd}i^{ab}i^{cs} + i^{ad}i^{rb}i^{cs})v_{st,u,b,c,d}(n^2)}_{O_p(n^{-2})} \\
&\quad + \underbrace{i^{bm}i^{cq}i^{tp}v_{lmn}v_{opq}\left(\frac{1}{4}r^{rl}i^{ao}i^{sn} + \frac{1}{2}i^{rs}r^{al}i^{on} + \frac{1}{2}i^{as}i^{rl}i^{on}\right)v_{s,t,b,c}(n^2)}_{O_p(n^{-2})} \\
&\quad + \underbrace{\frac{1}{2}i^{sm}v_{lmn}(i^{tn}i^{cd}(i^{rl}i^{ab} + i^{al}i^{rb}) + 2i^{bn}i^{cd}(i^{rl}i^{at} + i^{al}i^{rt}) + i^{cl}i^{tn}(i^{rd}i^{ab} + i^{ad}i^{rb}))v_{s,t,b,c,d}(n^2)}_{O_p(n^{-2})} \\
&\quad + \underbrace{\frac{1}{6}i^{mb}i^{nc}i^{od}v_{lmno}(i^{rs}i^{la} + i^{as}i^{rl})v_{s,b,c,d}(n^2) + 4i^{bm}(i^{rs}i^{al} + i^{as}i^{rl})v_{s,m,lb}(n^1)}_{O_p(n^{-2})} \\
&\quad - \underbrace{\frac{1}{4}i^{rs}i^{tu}i^{aw}i^{yz}v_{stu}v_{wyz} - i^{rs}i^{tu}i^{aw}i^{yz}v_{stu}v_{wyz}(n^1) - i^{rs}i^{tu}i^{aw}i^{yz}v_{st,u}(n^1)v_{wyz}(n^1)}_{O_p(n^{-2})}.
\end{aligned} \tag{3}$$

The notation $v_{bce,d,f,s}(n^2)$ indicates that in the joint moment $v_{bce,d,f,s}$ only polynomial terms of order n^2 are retained. The first-order covariance term of this expansion is simply the CRLB, and the sum of the other 10 terms provides the second-order variance. The ratio of this sum to the first-order variance (CRLB) is hereafter defined as the “second-to-first order variance ratio” (SFOVR), which is inversely proportional to sample size n . A necessary criterion for the MLE to attain minimum variance is for this ratio to become negligible. Note that this is only a *necessary* condition to attain minimum variance, and not a *sufficient* condition, because there is no guarantee that higher-order variance terms neglected in Eq. (3) will not exceed the second-order variance for sufficiently small n . For sufficiently large n , the series is guaranteed to converge if a minimum variance and unbiased estimate exists. In many practical scenarios the necessary conditions specified here are also sufficient for establishing optimality.

C. Gaussian data, deterministic, and random signals

The general bias and variance expressions of Eqs. (2) and (3) are now applied to the specific case of data that obey the conditional Gaussian probability density¹⁴

$$\begin{aligned}
p(\mathbf{X}; \boldsymbol{\theta}) &= \frac{1}{(2\pi)^{nN/2} |\mathbf{C}(\boldsymbol{\theta})|^{n/2}} \\
&\quad \times \exp \left\{ -\frac{1}{2} \sum_{j=1}^n (\mathbf{X}_j - \boldsymbol{\mu}(\boldsymbol{\theta}))^T \mathbf{C}(\boldsymbol{\theta})^{-1} (\mathbf{X}_j \right. \\
&\quad \left. - \boldsymbol{\mu}(\boldsymbol{\theta})) \right\}.
\end{aligned} \tag{4}$$

Here \mathbf{X}_i is one of n independent and identically distributed N -dimensional real-valued data vectors, and

$\mathbf{X} = [\mathbf{X}_1^T, \mathbf{X}_2^T, \dots, \mathbf{X}_n^T]$, \mathbf{C} is the real-valued covariance matrix, and $\boldsymbol{\mu}$ is the real-valued mean of the real random data. For the present study of underwater localization, \mathbf{X}_i represents the real and imaginary parts of the narrow-band acoustic data collected across an array of $N/2$ sensors around the given harmonic-source frequency, and the parameter set $\boldsymbol{\theta}$ represents the range and depth of the acoustic source. The fact that the number of hydrophones is half the length of the data vector \mathbf{X}_i follows from the use of this real vector to describe complex data as will be discussed in the next section.

In general both the data mean and covariance in Eq. (4) are functions of the desired parameter set $\boldsymbol{\theta}$, a situation that makes evaluation of the joint moments in Eqs. (2) and (3) difficult. Two limiting cases, however, are of great practical interest, since they describe a deterministic signal in additive noise and a completely randomized signal in noise, respectively. In the deterministic scenario the covariance matrix \mathbf{C} is independent of the parameter vector $\boldsymbol{\theta}$, while the mean $\boldsymbol{\mu}$ depends on $\boldsymbol{\theta}$. In the randomized scenario the sample covariance \mathbf{C} depends on $\boldsymbol{\theta}$ and the data mean $\boldsymbol{\mu}$ is zero. For this latter case the sample covariance of the data is thus a sufficient statistic that contains all information about the estimation parameters contained in the measured data.^{4,19}

Deterministic signals are typically measured in the presence of independent, additive noise in ocean acoustics. These deterministic signals may arise from narrow-band sources on seagoing vessels, or from deployed tomographic sources. A narrow-band time series from such a combination of signal and noise would have the form $z(t)\exp(i2\pi f_c t) + \xi(t)$, when measured at a single omni-directional receiver, where $\xi(t)$ is the independent, additive noise, $z(t)$ is a deterministic envelope, and f_c is the carrier frequency. The additive noise $\xi(t)$ typically arises from a large number of independent sources distributed over the sea surface.²⁰ These noise sources may be generated by wind, wave interactions, or ocean-going ves-

sels. Since the total noise field is the sum of large numbers of statistically independent contributions, it follows a Gaussian probability density, by virtue of the central limit theorem. The Gaussian probability density of Eq. (4) is then a valid representation of a deterministic signal embedded in additive noise.

The second limiting case explored here is for a fully randomized signal. A particular fully randomized Gaussian signal model that is very widely used and enjoys a long history in acoustics, optics, and radar is the circular complex Gaussian random (CCGR) model.²¹ A scalar signal centered around a carrier frequency f_c that obeys CCGR statistics would have the form $z(t)\exp(i2\pi f_c t) + \xi(t)$, where $\xi(t)$ is the independent, additive noise, and where $z(t)$ is an envelope whose real and imaginary parts are independent Gaussian random variables with zero mean, and equal variance. The instantaneous intensity of this signal thus obeys an exponential probability density function (PDF).^{22,23} In the radar literature the Swerling II model for radar returns from a fluctuating target is equivalent to the CCGR model, since the instantaneous intensity received in that case also follows an exponential PDF.^{23,24} There are many physical mechanisms for generating ocean acoustic signals with CCGR properties. Various types of mechanical and propeller noise generated by the complex source distribution of a ship or submarine generate incoherent source fluctuations that can be represented as a CCGR process in time. Even when the initial source signal is deterministic, natural disturbances in the waveguide, such as underwater turbulence or passing internal or gravity waves, lead to such randomness in the medium that the waveguide modes at the receiver can be treated as statistically independent entities. The total received field, which is the weighted sum of these modes, can then be modeled as a CCGR process in time. Randomized ocean acoustic signals have been modeled with CCGR statistics since World War II,^{22,25} and as a consequence the CCGR model has become a standard assumption for analyses of MFP performance.^{5,15,26,27}

Once C and μ have been obtained from either signal model, the joint moments are evaluated and inserted into Eqs. (2) and (3), to compute the asymptotic bias and covariance. The appropriate formulas for the joint moments are provided in Appendixes B and C in the companion paper,¹² for both deterministic and fully randomized signals, respectively.

III. WAVEGUIDE, SIGNAL AND NOISE MODELS

Four simple shallow-water ocean waveguide environments have been modeled to examine the effects of varying bottom composition and sound-speed profile on the bias and variance of a MLE for the location of an acoustic source.

Figure 1 displays the selected array geometry, sound speed profiles, and bottom composition for each environment. All simulations employ a 100 Hz monopole source at 50 m depth, and a 10-element vertical array with 7.5 m spacing, in a 100 m deep range-independent waveguide. The shallowest element lies at 16.25 m depth, so that the array is

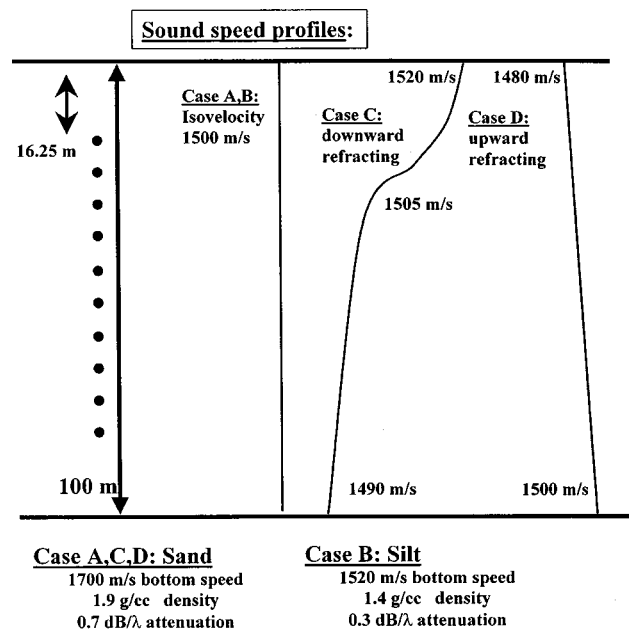


FIG. 1. Illustration of the ocean waveguide environments used in the paper. All cases employ a 100 m deep water column overlying a semi-infinite fluid half space, and a 10-element vertical array with 7.5 m spacing, with the first element positioned at 16.25 m depth. Cases A and B employ an isovelocity water profile of 1500 m/s (Pekeris profile). Case A uses geoacoustic parameters representative of a sand bottom, while case B uses parameters representative of a silt bottom. Case C uses the sand bottom, and a downward-refracting water sound-speed profile to simulate summer conditions in temperate latitudes. Case D is similar, except a linear upward-refracting profile is used to represent an arctic scenario.

centered in the waveguide. The ocean bottom is a fluid half space.

The first environment, case A, is a Pekeris waveguide with a bottom sound speed of 1700 m/s, a density of 1.9 g/cc, and an attenuation of 0.8 dB/wavelength, which are representative values for sandy environments.³ In case B, a silt bottom is simulated, using a bottom speed of 1520 m/s, density of 1.4 g/cc, and an attenuation of 0.3 dB/wavelength. Case C retains the sand bottom parameters, but uses a downward-refracting water sound-speed profile, measured during the Swellex-93 experiments^{28,29} conducted off the San Diego coast in 1993, under typical oceanic summer conditions in temperate latitudes.²⁹ Finally, case D illustrates the effects of propagation through an upward-refracting sound speed profile. The profile linearly decreases from 1500 m/s at the ocean bottom to 1480 m/s at the surface.

For ranges greater than a few ocean depths, the Green function for the acoustic field received by the m th hydrophone array element from a monopole source at horizontal range r and depth z at angular frequency ω can be expressed as a sum of normal modes³

$$\tilde{g}(z_m, z, r, \omega) = \frac{i e^{-i\pi/4}}{\rho(z) \sqrt{8\pi r}} \sum_l \Psi_l(z) \Psi_l(z_m) \frac{e^{ik_l r}}{\sqrt{k_l}}, \quad (5a)$$

where k_l is the horizontal wave number of mode l with modal amplitude $\Psi_l(z)$. Equation (5a) defines the m th element of the spatial vector $\tilde{\mathbf{g}}$ for $m = 1, 2, 3, \dots, N/2$, where $N/2$

is the number of hydrophones in the receiving array. For a source with amplitude $A_j(\omega)$, the j th sample or snapshot of the received field measured across the entire hydrophone array is comprised of the components of both a complex signal vector $A_j(\omega)\tilde{\mathbf{g}}$ and an additive CCGR noise vector $\tilde{\boldsymbol{\eta}}_j$ such that

$$\mathbf{X}_j = \begin{bmatrix} \text{Re}(A_j(\omega)\tilde{\mathbf{g}}) \\ \text{Im}(A_j(\omega)\tilde{\mathbf{g}}) \end{bmatrix} + \boldsymbol{\eta}_j \quad (5b)$$

for $j = 1, 2, 3, \dots, n$ where

$$\mathbf{g} = \begin{bmatrix} \text{Re}(\tilde{\mathbf{g}}) \\ \text{Im}(\tilde{\mathbf{g}}) \end{bmatrix}, \quad \boldsymbol{\eta}_j = \begin{bmatrix} \text{Re}(\tilde{\boldsymbol{\eta}}_j) \\ \text{Im}(\tilde{\boldsymbol{\eta}}_j) \end{bmatrix}, \quad (5c)$$

and \mathbf{X}_j are real vectors of length N . In the deterministic signal model $A_j(\omega)$ is a constant $A(\omega)$, for all j . In the random signal model the $A_j(\omega)$ are independent and identically distributed CCGR variables that describe a stationary random process where $\langle A_j(\omega) \rangle = 0$ and $\langle |A_j(\omega)|^2 \rangle = \langle |A(\omega)|^2 \rangle$ for $j = 1, 2, 3, \dots, n$.

The portion of the covariance matrix due to additive background noise for a single sample $n = 1$, or a single snapshot, of data across the vertical array is assumed to be spatially white, since this is typically what is measured in continental shelf environments,

$$\tilde{\mathbf{C}}^{\text{additive}} = \langle \tilde{\boldsymbol{\eta}}_j \tilde{\boldsymbol{\eta}}_j^+ \rangle - \langle \tilde{\boldsymbol{\eta}}_j \rangle \langle \tilde{\boldsymbol{\eta}}_j^+ \rangle = \sigma^2 \mathbf{I}, \quad (6)$$

where \mathbf{I} is the identity matrix, σ^2 is the instantaneous variance of the additive noise on each hydrophone and the $+$ superscript represents a Hermitian transpose. Computations using the spatially correlated Kuperman and Ingenito waveguide noise model³⁰ for the given environments are not shown here, but produce results similar to those derived from Eq. (6) since the theory predicts weak spatial correlation.

In general, for a properly defined SNR, terms in Eqs. (2) and (3) that are of order n^{-m} must also be of order SNR^{-m} . In the matched field processing literature, the signal to additive noise ratio (SANR) is typically used, which is not necessarily the SNR nor is it necessarily proportional to the SNR. For a single sample, $n = 1$, we define the SANR as

$$\text{SANR}[1]_{z_s, r} = \frac{\sum_{u=1}^{N/2} \langle |A(\omega)|^2 \rangle |\tilde{g}(z_u, z_s, r, \omega)|^2}{\text{trace}(\tilde{\mathbf{C}}^{\text{additive}})} \quad (7)$$

which is a function of source range r and depth z . For multiple independent and identically distributed samples in the deterministic signal model, $\text{SANR} = n \text{SANR}[1]$, for a given source range and depth. Moreover, terms in Eqs. (2) and (3) that are of order n^{-m} are also of order SANR^{-m} when the additive noise is zero-mean Gaussian and spatially *uncorrelated*, in the deterministic signal model, as shown in appendix B. This is not the case when the noise is spatially *correlated*. In the correlated case, terms in Eqs. (2) and (3) must be expanded in powers of a more generalized quantity that cannot simply be factored into the ratio of a signal term and a noise term. The tenant that SANR and SNR should conform to such a factorable ratio must be abandoned in this more generalized framework.

For a completely randomized signal in additive noise, the SANR and SNR are not equal, however, for consistency we still define $\text{SANR} = n \text{SANR}[1]$ in this case. Consider, for example, the case of a scalar measurement of a randomized signal with no additive noise. Here the SNR is independent of signal intensity because the variance of an instantaneous intensity measurement equals the square of the expected intensity. The SNR, which is the ratio of these two quantities, is unity for an instantaneous intensity measurement.²² The SANR of this same signal, however, is infinite, because no additive noise is present. More generally, for finite time measurements of intensity, the SNR for a scalar measurement of a completely randomized signal is defined as the ratio of the square of the expected intensity to the variance of this intensity, as has been described in detail in Refs. 22 and 19. Under such circumstances the SNR is then approximately equal to the number of independent samples n in a measurement time T where asymptotic convergence to n occurs for $n \gg 1$. For measurement times much greater than the coherence time τ_c for fluctuations in the received field, n is well approximated by T/τ_c .^{19,21,22} The number of fluctuations n is also equivalent to the time-bandwidth product of the received signal, where the bandwidth of the fluctuating field is $1/\tau_c$ in the limit as $T \gg \tau_c$.

For example, if a fast-Fourier transform (FFT) is applied to a data segment from a completely randomized signal of duration T , the effective number of independent samples n is T times the signal bandwidth, which is another way of stating that the signal is expected to fluctuate n times during the measurement. If T is much shorter than the coherence time τ_c of the random signal, then this measurement represents a single statistical sample where $n = 1$.

While the SANR has traditionally been the quantity of practical interest in MFP, the difference between SANR and SNR is important because a signal with high SANR might still have low SNR, due to signal-dependent fluctuations during measurements with low time-bandwidth products. All the randomized signal examples in this paper are computed for an instantaneous measurement, where $n = 1$ and the SNR is 1. Measuring the data over longer periods leads to a linear increase in the sample size n if the signal is deterministic or a nearly linear increase in n which is asymptotically linear for $n \gg 1$ if the signal can be described as a CCGR process.

Since SANR is a function of both source range and depth, for consistency, we adopt the convention of setting the $\text{SANR}[1]$ of the field across the array to unity for a source located at $r = 1$ km range and any depth z for all simulations presented in this paper. This implies that the SANR is made constant over source depth for any fixed range separation between the source and receiver array by appropriately varying the source amplitude with source depth.

We define the complex mean $\tilde{\boldsymbol{\mu}}$ and covariance $\tilde{\mathbf{C}}$ that are related to the real mean $\boldsymbol{\mu}$ and covariance \mathbf{C} of Eq. (4) by the following expressions:¹⁴

$$\boldsymbol{\mu} = \begin{bmatrix} \text{Re}(\tilde{\boldsymbol{\mu}}) \\ \text{Im}(\tilde{\boldsymbol{\mu}}) \end{bmatrix}, \quad \mathbf{C} = \frac{1}{2} \begin{bmatrix} \text{Re}(\tilde{\mathbf{C}}) & -\text{Im}(\tilde{\mathbf{C}}) \\ \text{Im}(\tilde{\mathbf{C}}) & \text{Re}(\tilde{\mathbf{C}}) \end{bmatrix} \quad (8)$$

which are valid under the assumption that the complex data measured at each hydrophone follow a circularly complex Gaussian random density²¹ when the mean is subtracted.

When modeling deterministic signals, the complex mean vector becomes $\tilde{\boldsymbol{\mu}} = A(\omega)\tilde{\mathbf{g}}$, and the complex covariance matrix $\tilde{\mathbf{C}}$ is taken to be $\tilde{\mathbf{C}}^{\text{additive}}$, for a single sample $n = 1$.

When modeling randomized signals due to random source amplitude $A_j(\omega)$, $\tilde{\boldsymbol{\mu}}$ is set to zero, and $\tilde{\mathbf{C}}$ is defined for a single sample $n = 1$ as

$$\tilde{\mathbf{C}} = \langle |A(\omega)|^2 \rangle \tilde{\mathbf{g}}\tilde{\mathbf{g}}^+ + \tilde{\mathbf{C}}^{\text{additive}}. \quad (9)$$

It is noteworthy that $\tilde{\mathbf{C}}^{-1}$ becomes singular when the additive noise vanishes in the random signal model given by Eq. (9) when $\tilde{\mathbf{g}}$ is *not* a scalar. For sufficiently high SANR, the error in estimating range and depth from *nonscalar* measurements of a randomized signal then approaches zero as the additive noise approaches zero, as is shown in Appendix B. If the signal randomness is due to fluctuations in the waveguide rather than at the source, Eq. (9) is not an appropriate model. A more appropriate model would replace $\tilde{\mathbf{g}}\tilde{\mathbf{g}}^+$ in Eq. (9) with a diagonal matrix that has the same diagonal elements as $\tilde{\mathbf{g}}\tilde{\mathbf{g}}^+$, as might arise from equipartition of modes in a fully saturated waveguide.^{19,22} This random signal model due to waveguide fluctuations would be well defined even in the absence of additive noise.

Note that the definition presented in Eq. (7) does not account for potential improvements in the SANR from array gain, which is $10 \log(N/2)$ for the ideal case of a plane wave signal embedded in spatially uncorrelated white noise. The 10-element array modeled here could then have an “array-gain-augmented SANR” that is up to 10 dB greater than that indicated by Eq. (7) for the given array. For this reason, it will sometimes be necessary to distinguish the SANR of Eq. (7) as “input SANR” as opposed to “array-gain-augmented SANR.”

In the given signal models, evaluation of Eqs. (2) and (3) requires knowledge of the higher-order derivatives of \mathbf{g} with respect to parameters r and z . The normal-mode depth derivatives must be computed to obtain the Green function depth derivatives. Since numerical differentiation of the modes can lead to instabilities, the modes at a given source depth are decomposed instead into upward and downward-propagating plane waves, so that depth derivatives can be derived by analytic differentiation. This procedure is discussed in detail in Appendix A.

If source amplitude is sought as well as source position, a three-dimensional parameter estimation problem must be solved. However, as shown in Appendix B, the additional uncertainties introduced by estimating the source amplitude do not noticeably affect the localization performance of either deterministic or randomized signals. One reason behind this is that the source amplitude parameter $A(\omega)$ for the standard monopole source assumed in MFP^{3,5,28} is linearly related to the measured data, which in this case is the complex pressure field across the array. Because the second-order derivative of the measurement with respect to amplitude is zero, many of the higher-order joint moments that appear in

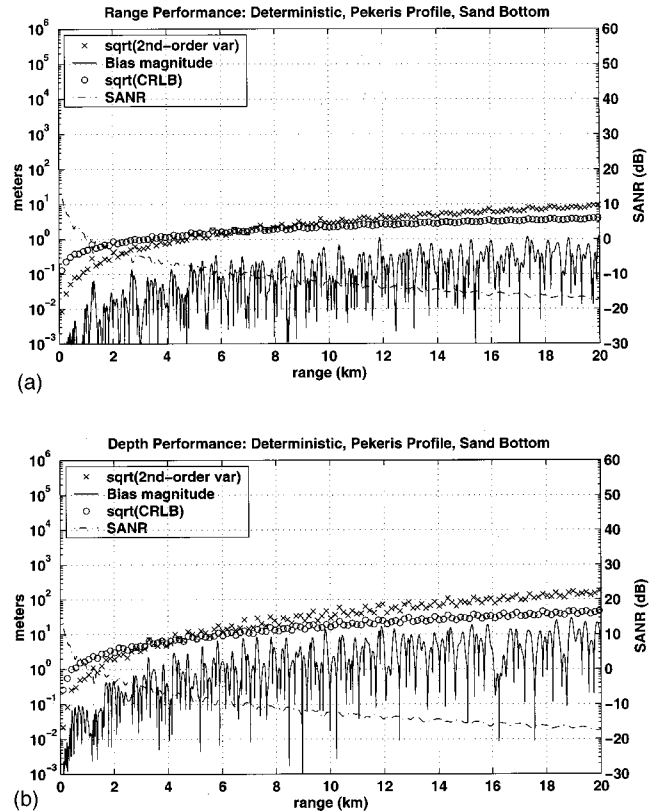


FIG. 2. Deterministic ocean acoustic localization MLE performance for (a) range estimation and (b) depth estimation versus source range, for a 100 Hz source placed at 50 m depth in the case A environment, a Pekeris waveguide with a sand bottom. The first-order bias magnitude (solid line), the square root of the Cramer–Rao lower bound (circles), the square root of the second-order variance (crosses), and the average input signal-to-additive noise ratio (SANR, dashed–dotted line) into the array are shown. Note that the input SANR plotted here does not incorporate array gain effects. All quantities are expressed in units of meters, except for the SANR, which is plotted in dB units. The background noise level has been scaled so that the input SANR is 0 dB at 1 km source range. Whenever the second-order variance attains roughly 10% of the CRLB, the total variance of the estimate will not attain the CRLB.

Eq. (2) and Eq. (3) are zero, and those that remain do not noticeably alter the localization estimates, as illustrated in the Appendix B figures.

IV. ILLUSTRATIVE EXAMPLES

The asymptotic biases and variances depend on the source signal characteristics, measurement geometry, SANR and SNR, and surrounding propagation environment. To isolate and illustrate these contributions, a number of simulations are performed. First, the source level and source depth are held fixed, and the first-order bias and second-order variance are computed as a function of source–receiver range for various waveguide environments, using both deterministic and randomized signals. Localization estimates are shown to degrade rapidly as (10 log of) the array-gain augmented SANR descends below 0 dB. (When SANR or SNR are discussed in decibels, 10 log of SANR is assumed.) Next, the minimum sample size necessary for the MLE to attain the CRLB is computed. A fundamental difference between the sample size requirements for randomized and deterministic

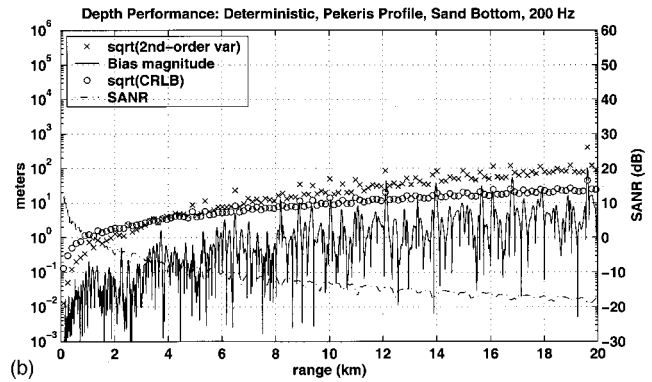
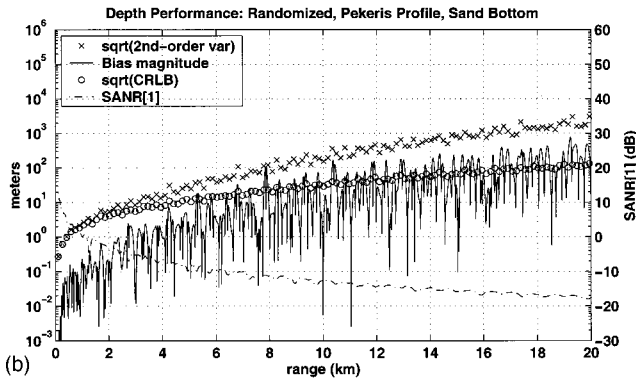
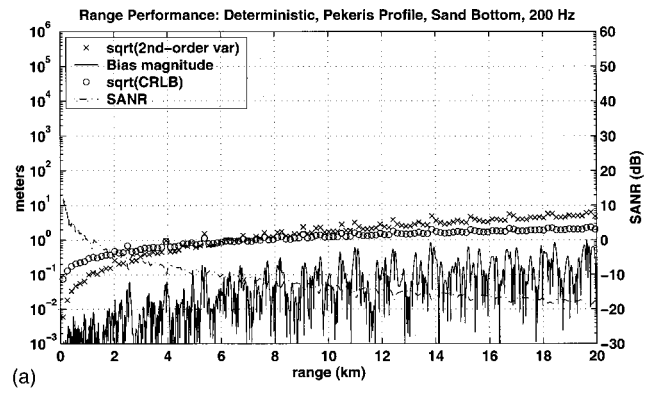
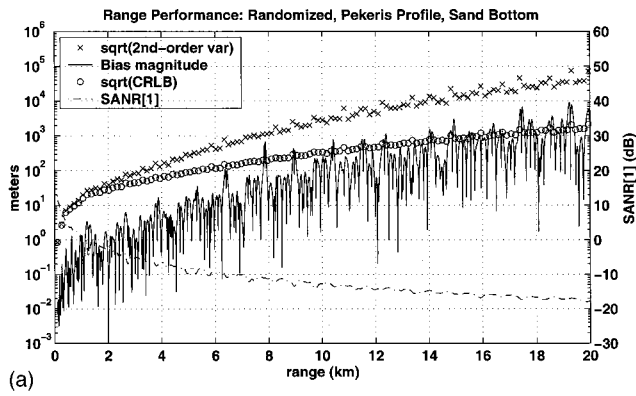


FIG. 3. Same as Fig. 2, recomputed for a single sample ($n=1$) of a completely randomized signal.

FIG. 4. Same as Fig. 2, except the deterministic source signal now radiates at 200 Hz.

signals is demonstrated. Finally, the spatial structures of the asymptotic bias and variance are investigated. It is shown that range and depth estimates tend to be biased toward certain waveguide locations as the array-gain augmented SANR falls below 0 dB.

In all cases where the deterministic signal model is used, the bias and variance terms are plotted as a function of $\text{SANR} = n\text{SANR}[1]$, since these terms are all proportional to SANR^{-m} , as shown in Appendix B, where m is the integer order of the term, i.e., m is either 1 or 2 in the illustrative examples. In all cases where the random signal model is used, the bias and variance terms are plotted as a function of $\text{SANR}[1]$, since these terms depend on n and $\text{SANR}[1]$ in different ways, as discussed in Appendix B. Since in both the deterministic and random signal models, the bias and variance terms always depend on n^{-m} , where m is the integer order of the term, all one must do to obtain a result for arbitrary n in any of these figures is to shift the curve according to the power m of the term involved and the value of n desired for a given $\text{SANR}[1]$.

A. Localization performance versus range and waveguide environment

The magnitude of the first-order bias, the CRLB, and second-order variance typically follow an increasing trend as a function of source range in Figs. 2–11, where the source depth is fixed at 50 m, the frequency is 100 Hz, and the sample size is unity, $n=1$. The input SANR for the deterministic signal examples and $\text{SANR}[1]$ for the random signal examples, computed from Eq. (7), are shown as a

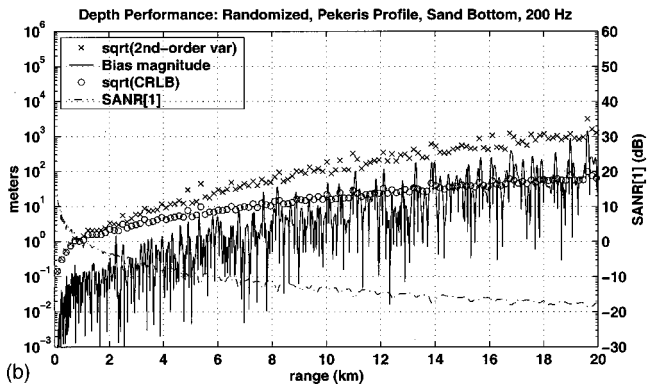
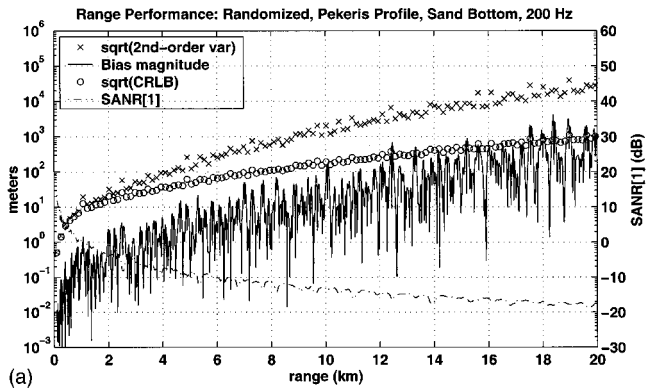


FIG. 5. Same as Fig. 3, except the randomized source signal now radiates at 200 Hz center frequency.

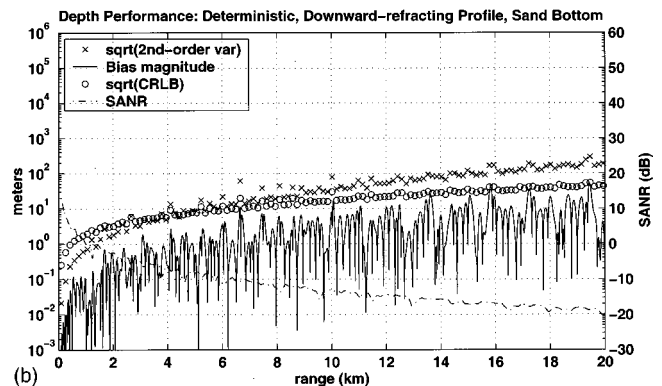
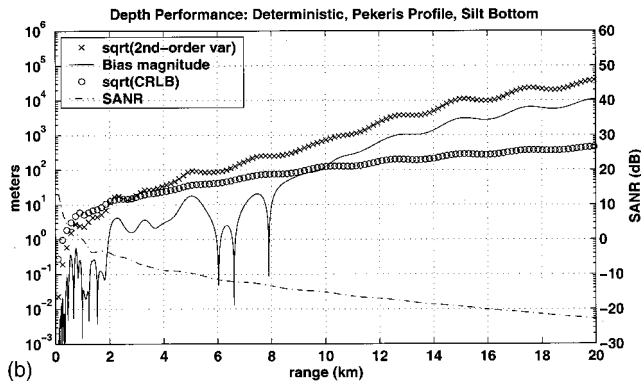
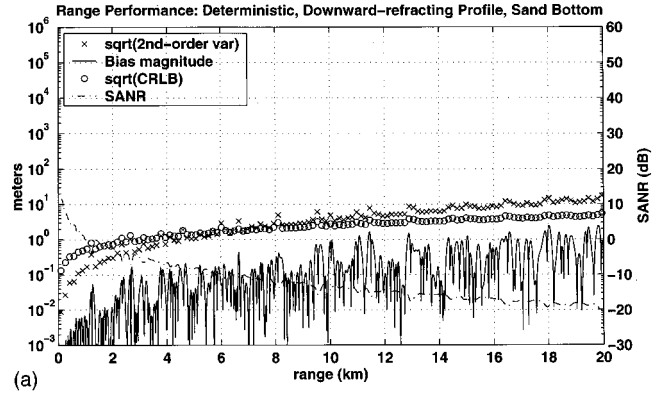
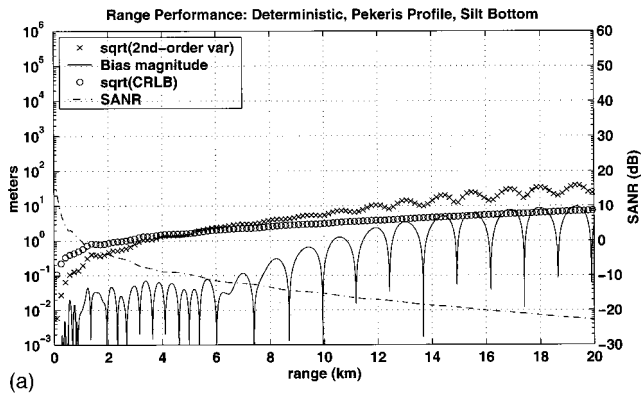


FIG. 6. Deterministic ocean acoustic localization MLE performance for (a) range estimation and (b) depth estimation versus source range, for a 100 Hz signal placed at 50 m depth in the case B environment, a Pekeris waveguide with a silt bottom. See Fig. 2 caption for plot descriptions.

FIG. 8. Deterministic ocean acoustic localization MLE performance for (a) range estimation and (b) depth estimation versus source range, for a 100 Hz signal placed at 50 m depth in the case C environment, which consists of a downward-refracting profile over a sand bottom. See Fig. 2 caption for plot descriptions.

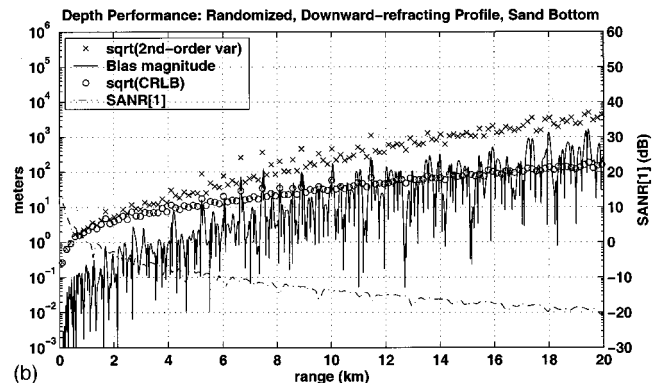
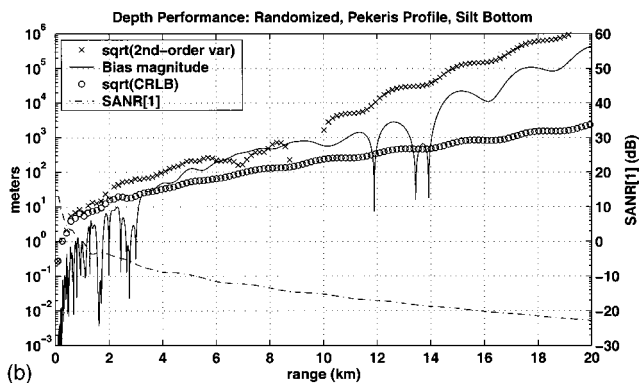
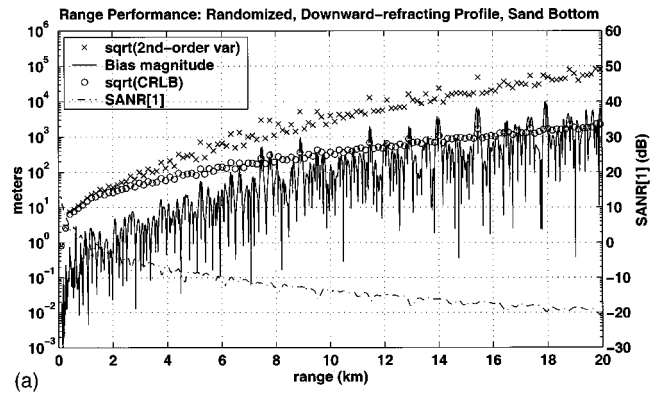
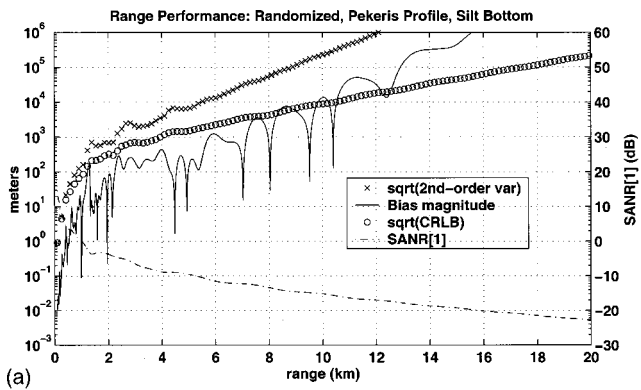


FIG. 7. Same as Fig. 6, recomputed for a single sample of a completely randomized signal.

FIG. 9. Same as Fig. 8, recomputed for a single sample of a completely randomized signal.

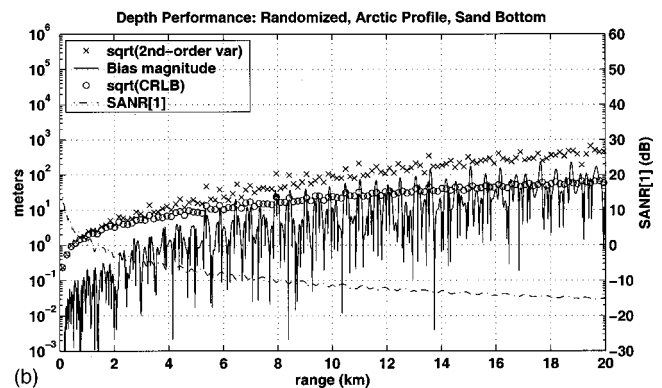
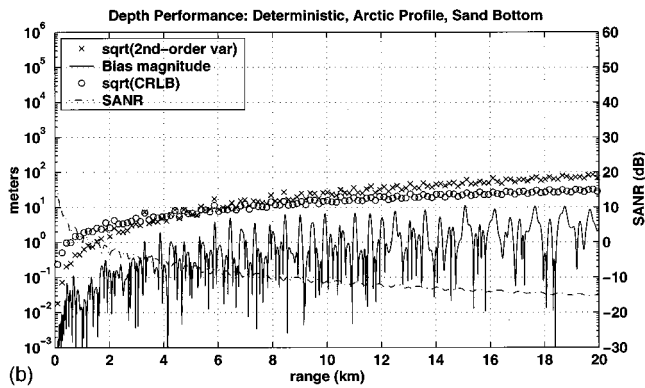
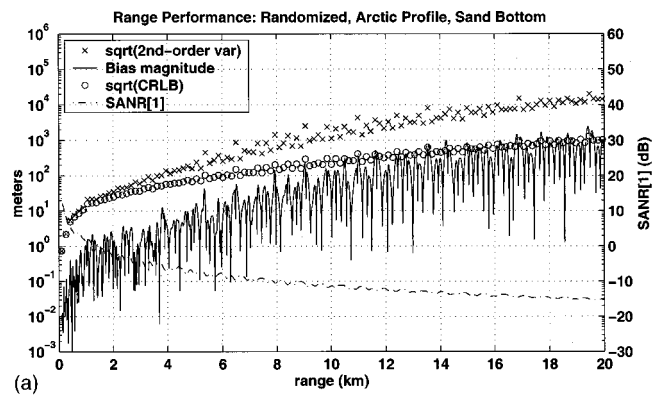
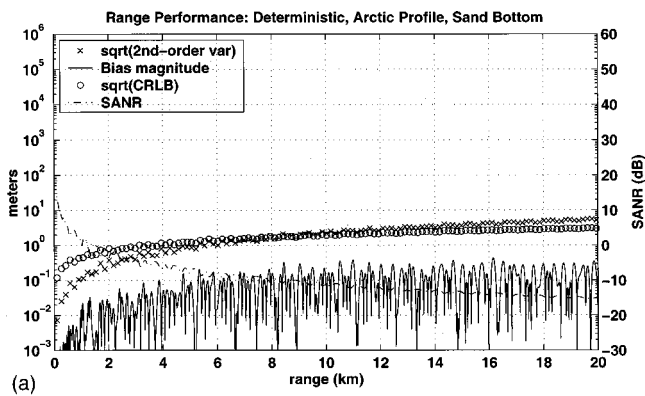


FIG. 10. Deterministic single-sample ocean acoustic localization MLE performance for (a) range estimation and (b) depth estimation versus source range, for a 100 Hz signal placed at 50 m depth in the case D environment, which consists of an upward-refracting profile over a sand bottom. See Fig. 2 caption for plot descriptions.

FIG. 11. Same as Fig. 10, recomputed for a single sample of a completely randomized signal.

dashed-dotted line plotted relative to the right vertical axis. In all figures the source level has been adjusted so that SANR or SANR[1] at 1 km is 0 dB. Note that it is the square root of the CRLB and the second-order variance that has been plotted in the figures.

Figures 2 and 3 show the results of propagation through the case A environment, which consists of an isovelocity sound speed profile over a sandy bottom. The randomized signal MLE biases are much larger than those from an equivalent deterministic signal and the degradation in the range estimation performance is especially notable. Hundreds to thousands of data samples are required to reduce the randomized bias to less than 10 m at 20 km range. At ranges less than 6 km, when the input SANR is greater than -10 dB, the range biases are negligible for deterministic signals, less than 1 m, but roughly 10 times more significant, 10 m, for randomized signals with SANR[1] greater than -10 dB at ranges of 6 km or less. For deterministic signals, as the input SANR descends below -10 dB, the bias magnitude increases by an order of magnitude, so that at 20 km range, where the input SANR drops to -19 dB, the asymptotic range and depth biases reach maxima of 1 and 30 m, respectively. The corresponding maxima for the randomized signal biases are 8000 m and 800 m, for a 20 km range source. Even at a typical operational range of 6 km, where the array-gain augmented SANR[1] is roughly 0 dB, the randomized signal localization biases are greater than 10 m.

A similar pattern is evident for the second-order vari-

ance. As the input SANR descends below -10 dB, the second-order variance magnitude grows much more rapidly than the CRLB magnitude, for both signal types. Beyond 6 km range the second-order localization variances of the deterministic signal equal or exceed those of the CRLB. For randomized signals, the second-order localization variances are even greater, exceeding the CRLB by nearly two orders of magnitude at 6 km range. In both cases the CRLB underestimates the true parameter variance, and tens to thousands of data samples are required to make the second to first-order variance ratio (SFOVR) negligible, and so have the MLE asymptotically attain minimum variance.

Figures 4 and 5 show the results of using a 200 Hz signal to estimate source position in the case A environment. One might expect the greater number of available propagating modes to improve the MLE localization performance. Indeed, the localization bias magnitude for both signal types decreases slightly. Doubling the frequency also reduces the range and depth second-order variance terms by factors of 4, for both signal types. However, the deterministic CRLB is also reduced by a similar factor. Therefore, while the localization variance decreases with increasing frequency, the SFOVR remains unaffected, so there is no reduction in the number of deterministic data samples required to attain the CRLB. In contrast, the randomized signal SFOVR does decrease with increasing frequency.

Figures 6 and 7 show the effects of a different bottom composition, in this case, silt, on the localization performance, using the original 100 Hz source. The localization performance has worsened noticeably relative to that of the sand bottom, due to the absence of higher-order modes. For

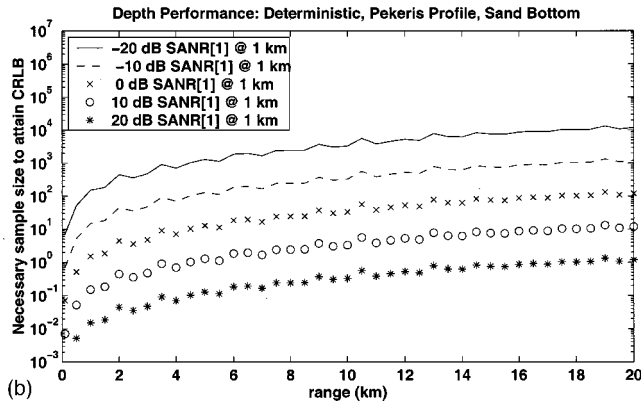
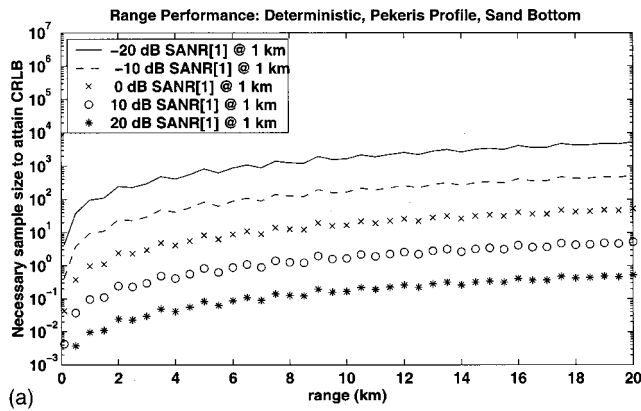


FIG. 12. Minimum independent data sample size (MSS) necessary for a deterministic ocean acoustic MLE to effectively attain the CRLB. The MSS is defined in Eq. (13) as the minimum sample size necessary for the second-order variance to be reduced to 10% of the CRLB. The MSS is plotted for (a) range estimation and (b) depth estimation versus source range and source level, for the case A environment. The 100 Hz source is located at 50 m depth. Values less than 1 indicate that a single data sample is sufficient to attain the CRLB.

example, the deterministic depth bias exceeds the 100 m waveguide depth beyond 9 km range, whereas for a signal propagating over a sand bottom, the bias is less than 100 m out to 20 km range. The randomized depth bias exceeds the waveguide depth beyond 5 km range in the silt environment, compared with 12–14 km for the sand environment. Even at typical operational ranges of a few kilometers, randomized signals received with an array-gain augmented SANR[1] of 0 dB will have range and depth biases on the order of tens of meters.

Figures 8–11 illustrate the effects of including the more complex sound speed profiles of cases C and D. A comparison between these figures and Figs. 2 and 3 suggests that the variations in the sound speed profile illustrated in Fig. 1 have relatively minor effects on localization performance, as compared with changes in bottom composition.

B. Minimum sample size necessary to attain CRLB

Figures 12–15 show the minimum sample sizes necessary for the second-to-first-order variance ratio (SFOVR) to be less than 0.1. We take this as a necessary condition for an MLE estimate to approximately attain the CRLB in the asymptotic regime. For convenience a necessary minimum

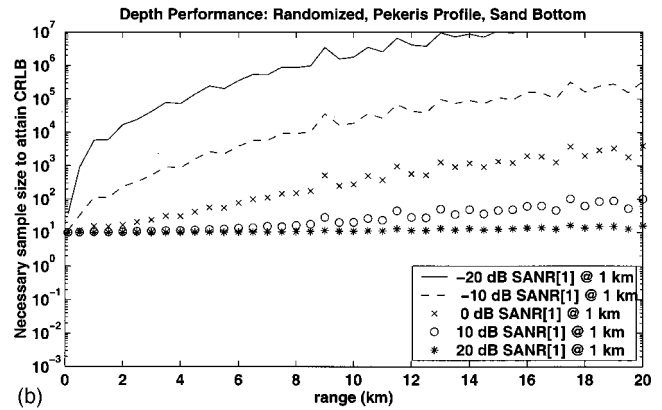
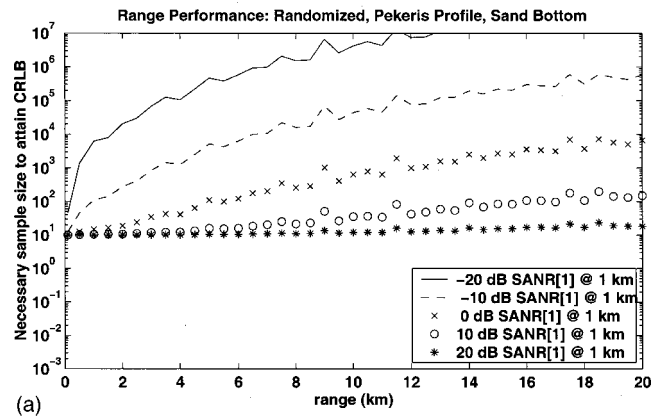


FIG. 13. Same as Fig. 12, recomputed for a completely randomized signal.

sample size (MSS) is defined here as 10 times the ratio of the second-to-first order variance for a single sample. In other words, if $\text{var}_1(n)$ represents the first-order variance term in Eq. (3), derived from n samples, and $\text{var}_2(n)$ represents the sum of all the second-order terms, also derived from n samples, then our necessary criterion becomes

$$\frac{\text{var}_2(n)}{\text{var}_1(n)} = \frac{\text{var}_2(1)}{n \text{var}_1(1)} \leq 0.1, \quad (10a)$$

where

$$\text{MSS} = 10 \frac{\text{var}_2(1)}{\text{var}_1(1)}. \quad (10b)$$

A single sample is sufficient to achieve the CRLB, for MSS values less than or equal to unity. The required MSS has been plotted as a function of range for the case A environment in Figs. 12 and 13, for both deterministic and randomized signals. For a deterministic signal with an input SANR of 0 dB at 1 km, as modeled in Fig. 2, an MSS of 20 is necessary to attain the CRLB at a range of 10 km and a depth of 50 m. If the input SANR increases by a factor of 10 (10 dB), only two samples would be required to attain the deterministic CRLB, since MSS is inversely related to SNR[1] and SANR[1] for deterministic signals, as discussed in Appendix B.

The randomized signal results in Fig. 13 display some fundamental differences from their deterministic counter-

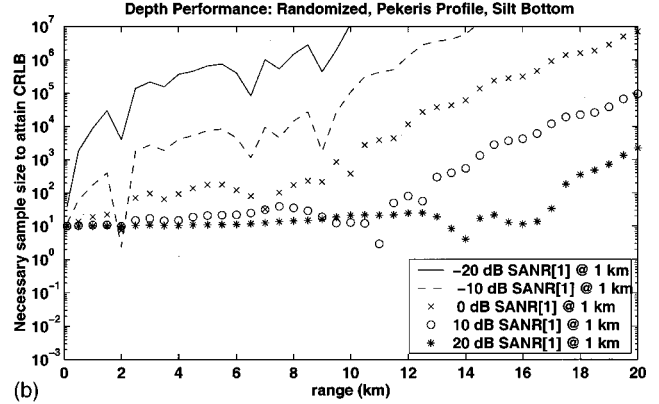
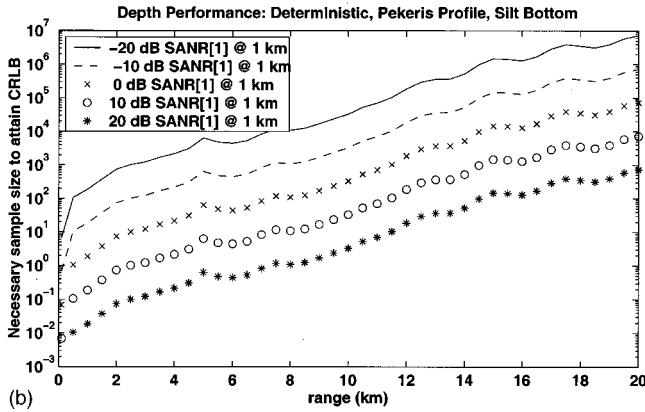
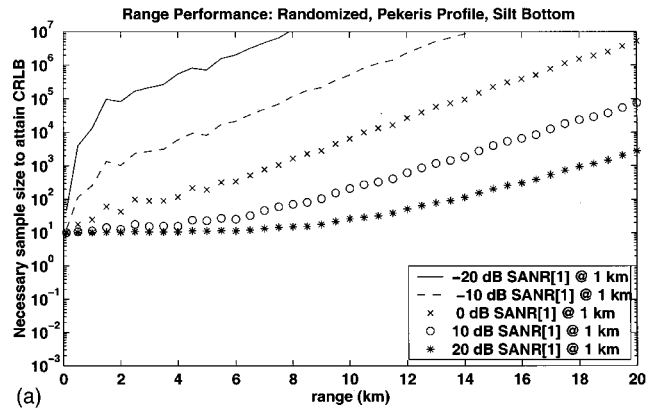
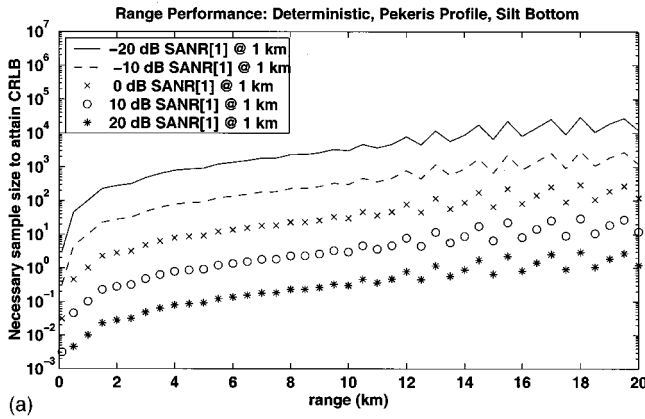


FIG. 14. Minimum independent data sample size necessary for a deterministic ocean acoustic MLE to effectively attain the CRLB for the case B environment. All other parameters remain unchanged from Fig. 12.

FIG. 15. Same as Fig. 14, recomputed for a completely randomized signal.

parts. First, the randomized MSS is always much larger than those required for deterministic signals. For example, roughly 1000 data samples are required to attain the CRLB at 10 km range and 50 m depth, for a signal with an input $\text{SANR}[1]$ of 0 dB at 1 km range. The randomized MSS eventually plateaus to approximately 10 as the $\text{SANR}[1]$ increases. Indeed, the MSS uniformly converges to a value of 10 at all ranges, as the $\text{SANR}[1]$ increases past 20 dB at 1 km range. In other words, the second-order variance converges to the same magnitude as the first-order variance at large $\text{SANR}[1]$ values. When the additive noise term is zero and $N/2 > 1$, however, the random signal model is not well defined as is discussed in Appendix B since the covariance given in Eq. (9) is no longer invertible.

Figures 14 and 15 show the MSS for deterministic and randomized signals, respectively, in the case B environment, a Pekeris waveguide with a silt bottom. While the MSS values are generally much greater than the values obtained for a signal propagating over a sand bottom, the overall trends visible in the MSS are the same as observed for the sand bottom. The deterministic signal MSS follows the expected inverse relationship with $\text{SNR}[1]$, and the randomized signal MSS asymptotically approaches 10 as the input $\text{SANR}[1]$ becomes large, converging $\text{SNR}[1]$ to 0 dB.

C. Effect of source depth on localization performance

Another factor that influences localization performance is the source depth. Figures 16 and 17 illustrate the CRLB,

bias magnitude, bias sign, and the MSS for a deterministic signal in the case A environment. As discussed in Sec. III, the noise matrix has been rescaled so that SANR from a 1 km range source will be 0 dB for every source depth. Figures 18 and 19 show the corresponding results for randomized signals in terms of $\text{SANR}[1]$.

The general features of the contour plots are similar for both signal types. As SANR follows a decreasing trend with range, both the CRLB and MSS increase together in a highly correlated fashion. Locations with a large CRLB also tend to require a large MSS to attain the bound. For a given source range in this environment, the waveguide center and boundaries tend to produce the lowest CRLB and MSS. In Fig. 17 only the depth bias displays any significant depth dependence, where it increases sharply near the waveguide boundaries. An examination of the depth bias sign of both signal types reveals that the large biases at the boundaries tend to shift the estimates toward the waveguide center, so that localizations near the surface will be positively biased, and localizations near the ocean bottom will be negatively biased.

The depth bias shows other sign reversals with depth, for both deterministic and randomized signals. The 100 Hz signal in the case A environment generates 11 distinct sign reversals over the waveguide depth, out to ranges of 5 km. Beyond this range the bias sign structure dissipates as the input SANR falls below -10 dB. The consequence of these

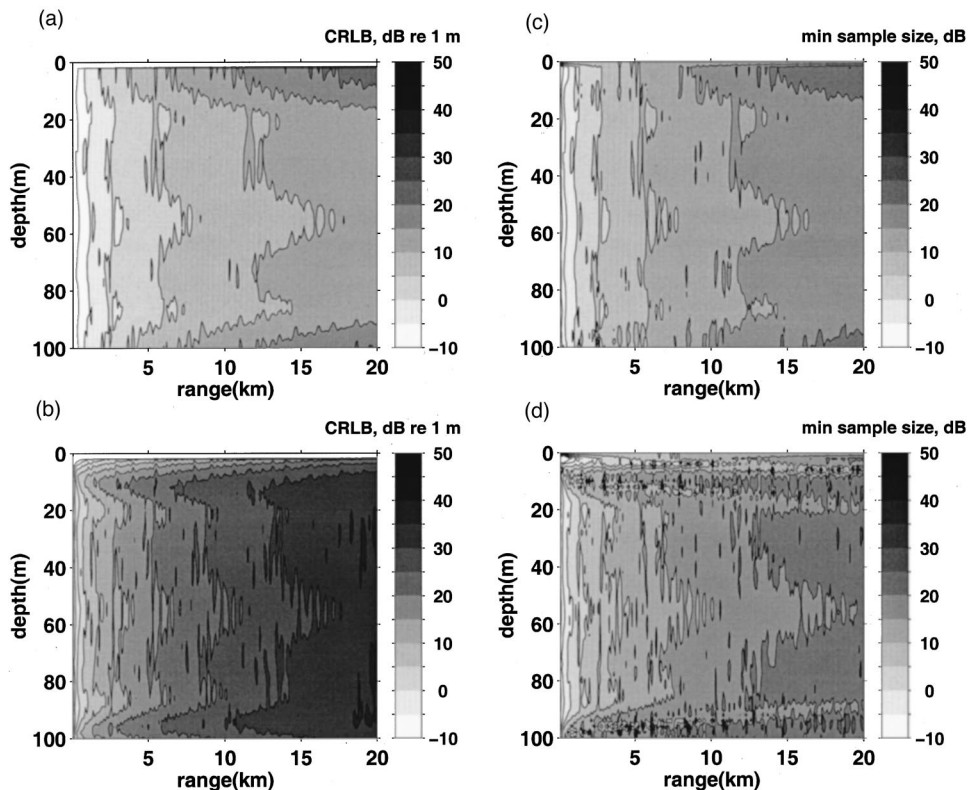


FIG. 16. Contour plots of (a) deterministic range CRLB, (b) deterministic depth CRLB, (c) minimum sample size required for a deterministic range estimate to attain the CRLB, and (d) minimum sample size required for a deterministic depth estimate to attain the CRLB. The 100 Hz acoustic source has been placed in the case A environment, and the received SANR at 1 km source range is 0 dB at all source depths, as described in Sec. III. All quantities are expressed in terms of dB units, and the contour interval is 5 dB *re* 1 m.

depth patterns is that MLE depth estimates will have a tendency to converge toward depths where the bias sign switches from positive to negative, with increasing depth. In terms of the contour plot, these regions lie wherever a black (positive bias) layer overlies a white (negative bias) layer. The range bias sign also shows alternating patterns indicative

of range convergence, particularly at the waveguide mid-depth.

These spatial effects are more dramatic when an environment with fewer propagating modes is analyzed. Figures 20–23 illustrate the results of applying the same asymptotic bias and variance computations to the case B environment,

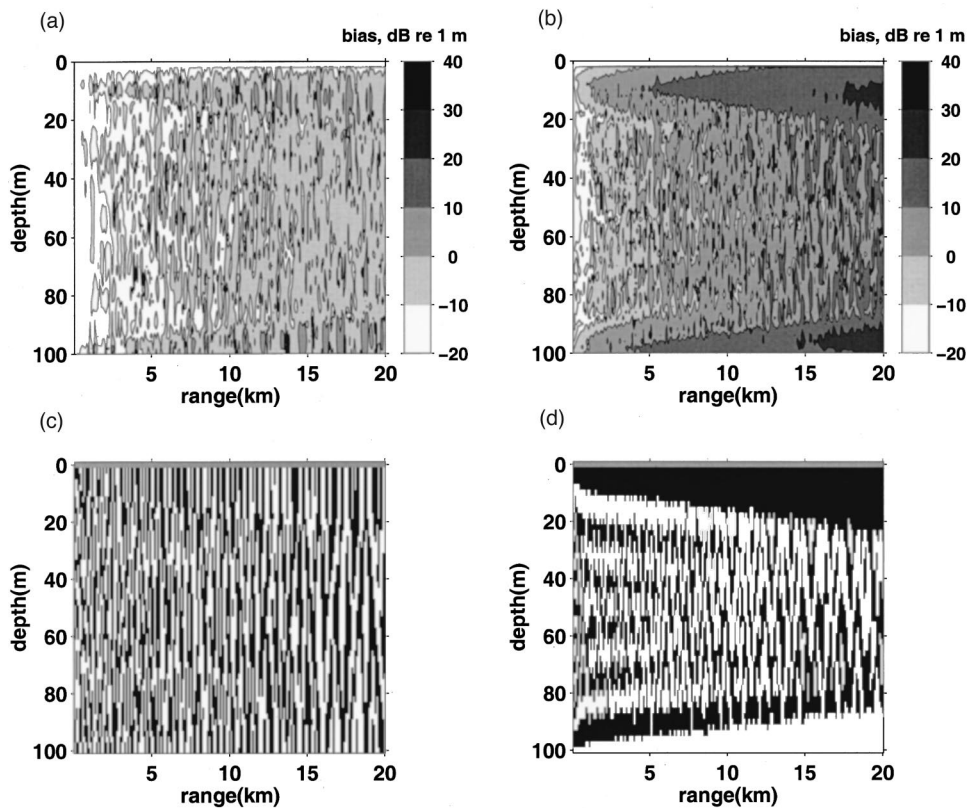


FIG. 17. Contour plots of (a) deterministic range bias magnitude, (b) deterministic depth bias magnitude, (c) deterministic range bias sign, and (d) deterministic depth bias sign, for the same scenario described in Fig. 16. The top row is in dB units, with a contour interval of 10 dB *re* 1 m. The bottom row displays positive values as black, negative values as white. Note the horizontal layers of alternating sign in the depth bias sign plot.

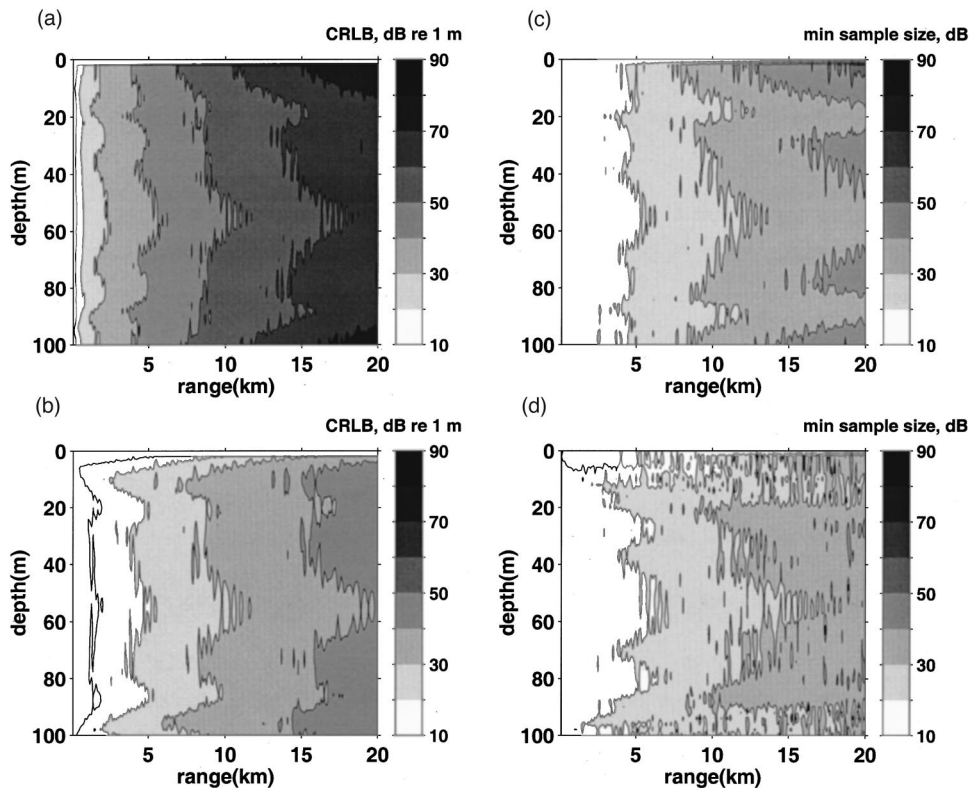


FIG. 18. Same as Fig. 16, recomputed for a completely randomized source signal. The contour interval is 10 dB.

characterized by a silt bottom. In both propagation environments depth localizations near the waveguide boundaries lead to the best performance, in terms of both the CRLB and MSS. For the silt case, the CRLB and MSS reach their maxima at the waveguide midpoint. The localization biases clearly display strong tendencies to converge at certain

ranges and depths. For example, deterministic signal localizations will tend to converge toward the waveguide mid-depth and toward range cells evenly separated 2.5 km apart, which is the modal interference length between the two propagating modes in the system. The randomized signal localizations display similar features.

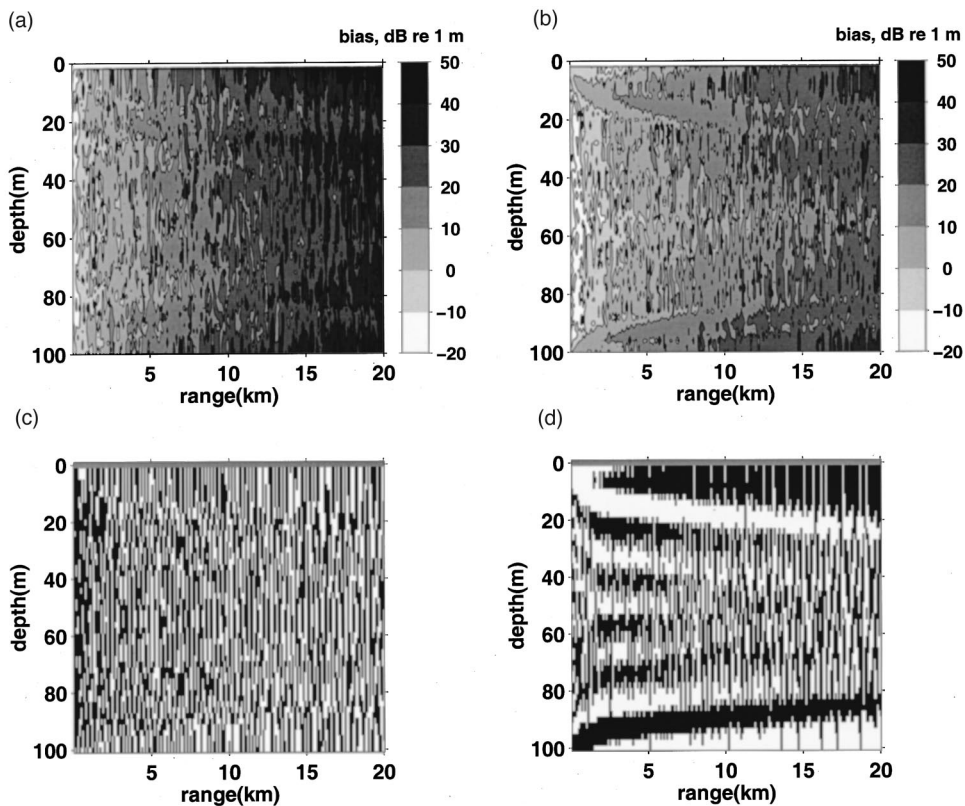


FIG. 19. Same as Fig. 17, recomputed for a completely randomized source signal. The contour interval for the top row is 10 dB *re* 1 m, and the bottom row displays positive values as black, negative values as white.

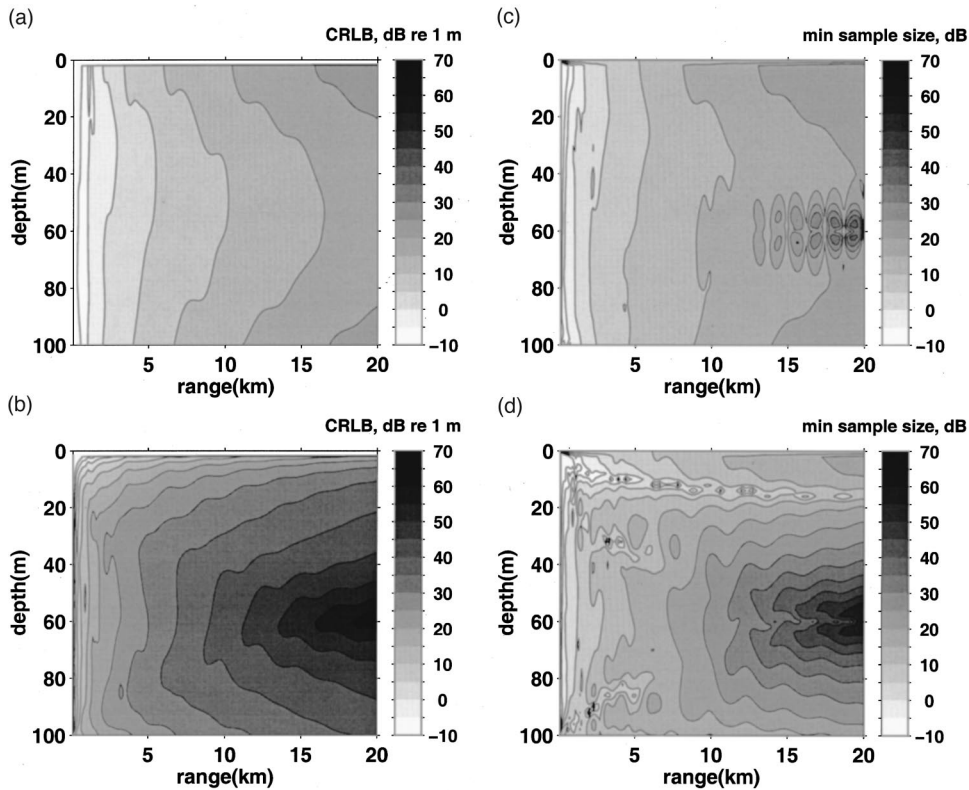


FIG. 20. Same as Fig. 16, but recomputed for a deterministic signal propagating through the case B environment. The contour interval is 5 dB.

V. DISCUSSION

It is convenient to frame the discussion in terms of SANR, starting in the high SANR regime. The results presented in Figs. 2–23 have been computed using a 10 element array. As indicated above, an increase in the number of array elements used to perform the inversion is expected to lead to

a reduction in the biases and variances presented here, due to the effects of array gain. In the presence of spatially uncorrelated white noise, an $N/2$ -element array increases the array-gain augmented SANR by $10 \log(N/2)$ over the input SANR defined in Eq. (7). Since the bias and variance have been shown to be primarily functions of the signal SNR, these

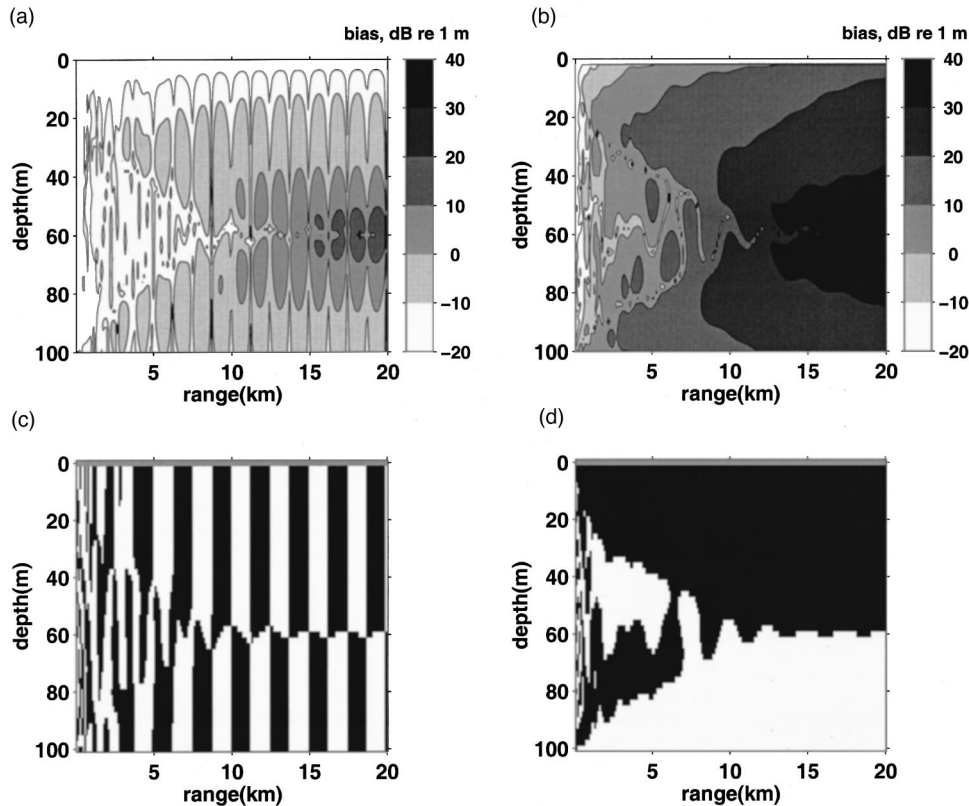


FIG. 21. Same as Fig. 17, but recomputed for a deterministic signal propagating through the case B environment. The contour interval for the top row is 10 dB re 1 m, and the bottom row displays positive values as black, negative values as white.

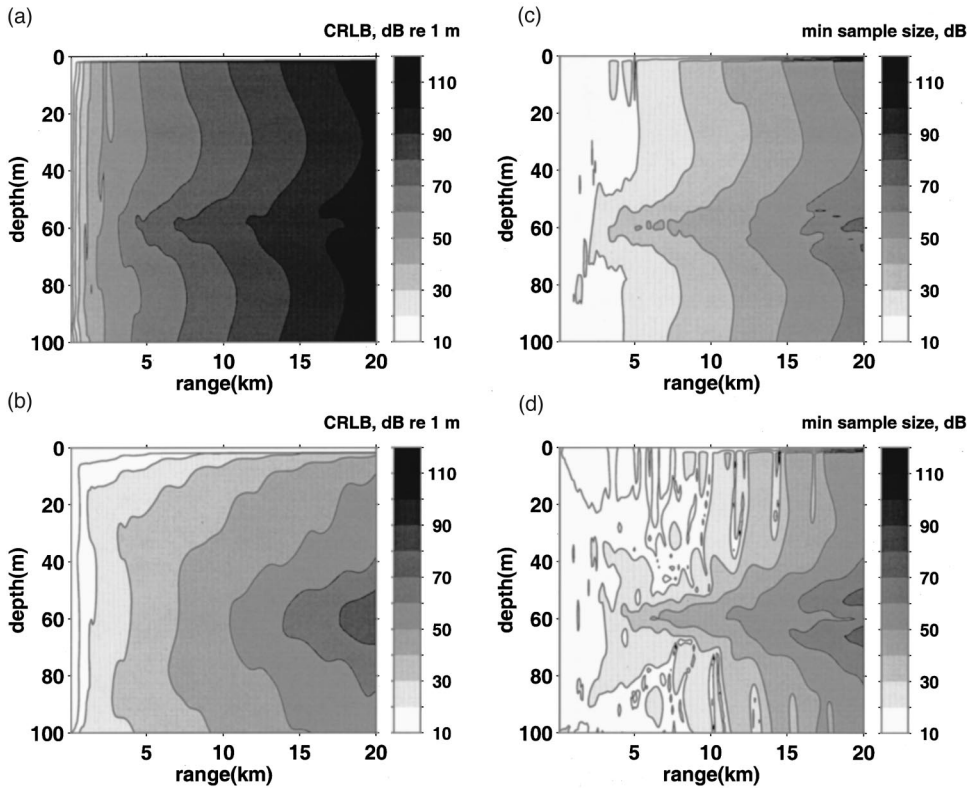


FIG. 22. Same as Fig. 16, but recomputed for a completely randomized signal propagating through the case B environment. The contour interval is 10 dB.

quantities decrease with increasing array gain. For example, a 10-fold increase in the number of hydrophone elements is expected to generate a 10-fold decrease in the deterministic bias and MSS, provided that the background noise covariance has similar characteristics to uncorrelated white noise.

Estimates extracted from deterministic signals can attain

the CRLB with a single sample or snapshot of the field across the array, for sufficiently high SANR values, as Figs. 12 and 14 attest. In other words, at high SANR levels the second-order variance computed from Eq. (3) is negligible relative to the first-order variance, even when $n=1$. However, Figs. 13 and 15 illustrate how the situation for ran-

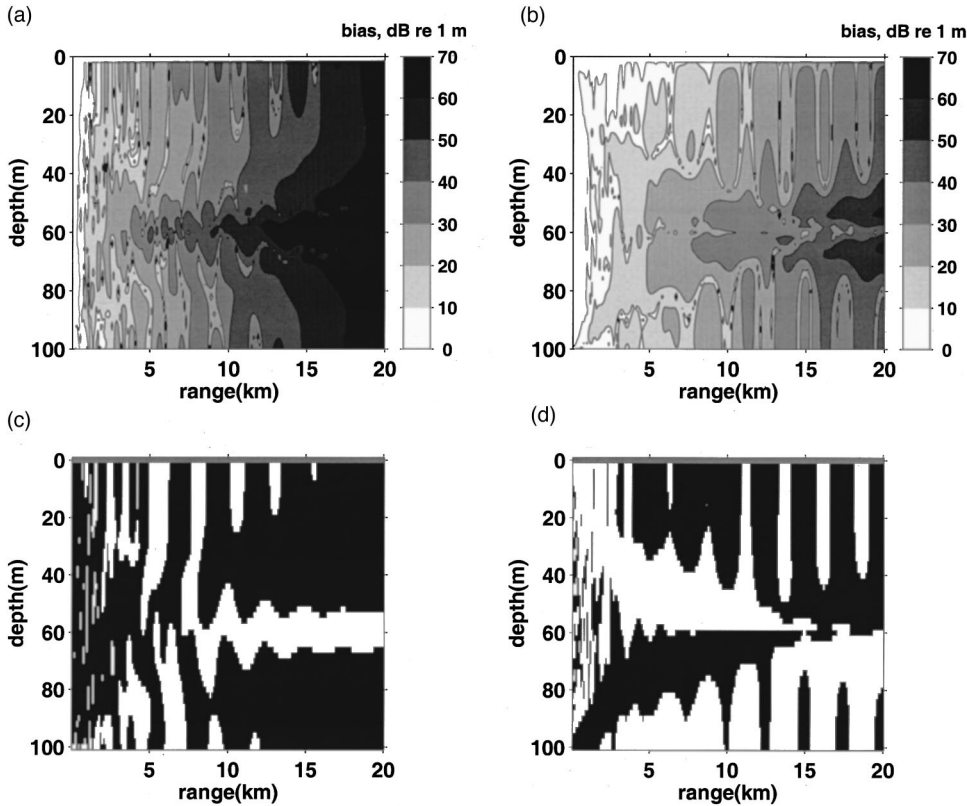


FIG. 23. Same as Fig. 17, but recomputed for a completely randomized signal propagating through the case B environment. The contour interval for the top row is 10 dB re 1 m, and the bottom row displays positive values as black, negative values as white.

domly fluctuating signals is more complex, in that estimates derived from these signals do not attain minimum variance, unless at least 10 data samples are used to construct the estimate. The reason behind this limitation is outlined in Sec. III, where the difference between the SANR, SANR[1] and the SNR of a measurement is discussed.

For example, Figs. 12 and 14 show that as the input SANR of a deterministic signal descends below -10 dB, the magnitude of the second-order variance begins to exceed the CRLB, so a deterministic estimate derived from a single data sample fails to attain the CRLB. As stated earlier, a -10 dB input SANR across a 10-element array yields an approximate array-gain augmented SANR of 0 dB.

For every 10 dB decrease in SANR, the deterministic SFOVR increases by an order of magnitude, resulting in a 10-fold increase in the MSS. This inverse relationship between the MSS and SANR[1] is a consequence of the fact that given spatially white noise in the deterministic signal model $\text{SNR} = \text{SANR} = n \text{SANR}[1]$, as discussed in Sec. III. The MSS itself is relatively insensitive to changes in source frequency, sound-speed profile, and even bottom composition, for the cases investigated. For example, a 6 km range source in a sandy environment yields the same input SANR (-10 dB) as a 4 km range source in a silt environment. Examination of Figs. 12 and 14 show that the MSS is the same for both situations, suggesting that the deterministic signal results presented here can be used to guide analysis in other propagation environments and array geometries, if the transmission loss curves are known.

No simple relationship between SANR[1] and MSS exists for randomized signals, because the SANR is not proportional to SNR in this case. As Figs. 13 and 15 demonstrate, the SFOVR, and thus the MSS, are nonlinearly related to SANR[1] and are very sensitive to propagation effects. Environments dominated by only a few propagating modes, in particular, seem to create situations where the SFOVR and MSS can change by an order of magnitude with only a small change in source range. However, at high SANR[1] levels the MSS asymptotically approaches a value of 10 at all ranges and for all environments investigated, which seems to imply that for $n=1$ the CRLB cannot be attained for large SANR[1]. Our analysis indicates that this is only the case when $\frac{n}{2}=1$ because for more than one receiver the error tends to zero for large SANR[1] as is discussed in Appendix B. This asymptote is due to the fact that with our definition of SANR[1], in the random signal model terms in Eqs. (2) and (3) that are of order n^{-m} are not necessarily also of order $\text{SANR}[1]^{-m}$. Both 1st and 2nd order terms may then approach zero with the same power law in SANR[1].

As the array-gain augmented SANR descends below 0 dB the localization biases are no longer negligible for either signal type. The spatial distribution of the bias sign reveals that the maximum-likelihood localization estimates tend to converge toward particular ranges and depths at low SANR. The exact convergence locations depend on the propagation environment; however, the localizations are generally biased away from the waveguide boundaries.

In some sense, the results provided here are still optimistic, as the ocean environment has been assumed perfectly characterized. In most practical situations, the waveguide parameters are insufficiently known, and this environmental uncertainty will further degrade the localization performance. The effects of this environmental uncertainty can be incorporated into Eqs. (2) and (3) by adding geoacoustic parameters to the parameter vector θ , and then computing derivatives of Eq. (5) with respect to these parameters. This differentiation may be accomplished either via numerical methods or by perturbation theory.³¹

VI. CONCLUSION

Asymptotic expressions for the first-order bias and second-order variance of a MLE have been applied to the problem of localizing an acoustic source in an ocean waveguide, for the cases of deterministic and randomized signals received with independent and additive background noise. The results suggest that as the array-gain augmented signal-to-additive noise ratio (SANR) at the array output descends below 0 dB, the MLE exhibits significant biases and variances that can exceed the CRLB by orders of magnitude. The localization biases tend to concentrate the estimates around particular source ranges and depths for moderate SANR values.

In principle, if enough data samples are available, unbiased estimates can be derived from low SANR signals. However, if the acoustic source is changing position with time, as is usually the case, the number of independent data samples available to construct a localization estimate is limited, because the estimation parameters themselves are changing with time. Therefore, under many practical operational scenarios, localization estimates are expected to be significantly biased, and the CRLB will underestimate the true variance by orders of magnitude.

ACKNOWLEDGMENT

This research was sponsored by ONR.

APPENDIX A: ANALYTICAL DERIVATIVES OF MODES USING PLANE-WAVE DECOMPOSITION

The moments presented in Appendixes B and C in paper I¹² require expressions for multiple-order depth derivatives of the waveguide normal modes. These are achieved by decomposing an individual mode into an upward and downward propagating plane wave at the desired source depth. Suppose that the values of mode Ψ_m at depths z and $z+H$ are known, where H is a small depth increment. Assuming that the sound-speed is constant between the two depths, the coefficients of the upgoing and downgoing plane waves connecting the two points are obtained by a matrix equation:

$$\begin{bmatrix} \Psi_m(z) \\ \Psi_m(z+H) \end{bmatrix} = \begin{bmatrix} 1 & 1 \\ e^{ik_{m,z}H} & e^{-ik_{m,z}H} \end{bmatrix} \begin{bmatrix} A^+ \\ A^- \end{bmatrix}, \quad (\text{A1})$$

where $k_{m,z} = \sqrt{k^2 - k_{r,m}^2}$ is the vertical modal wave number. The above matrix is easily inverted to solve for the coeffi-

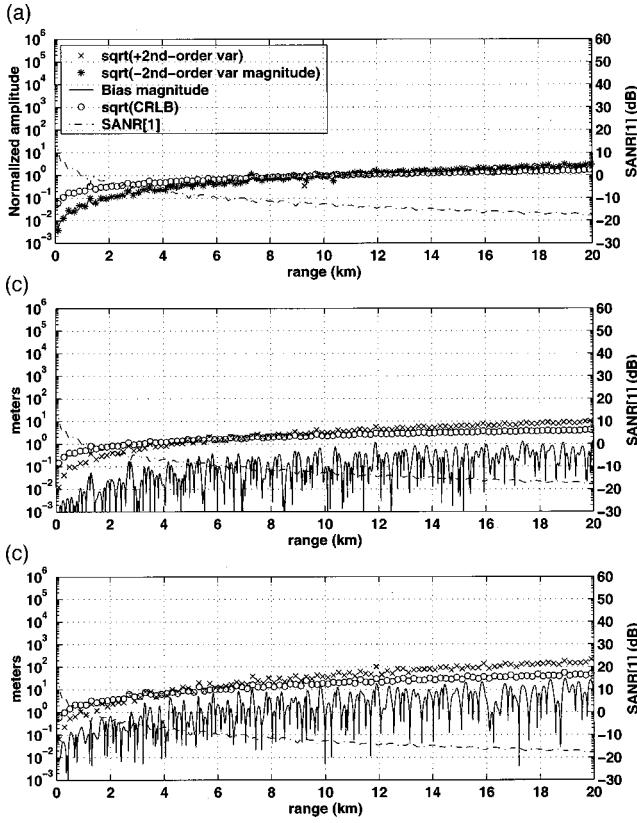


FIG. 24. Deterministic signal single-sample ($n=1$) ocean acoustic MLE performance for (a) amplitude A , (b) range, and (c) depth estimation versus source range, for a 100 Hz signal placed at 50 m depth in the case A environment, a Pekeris waveguide with a sand bottom. The true source amplitude A is 1. A comparison of these results with Fig. 2 shows that the addition of amplitude as an estimation parameter has negligible effect on the MLE localization performance.

cient vector \mathbf{A} . The modal derivatives with respect to depth can then be written in terms of \mathbf{A} :

$$\begin{aligned} \mathbf{U}_z &= \begin{bmatrix} \Psi'_m(z) \\ \Psi'_m(z+H) \end{bmatrix} \\ &= \begin{bmatrix} ik_{m,z} & -ik_{m,z} \\ ik_{m,z}e^{ik_{m,z}H} & -ik_{m,z}e^{-ik_{m,z}H} \end{bmatrix} \begin{bmatrix} A^+ \\ A^- \end{bmatrix} \\ &\equiv \mathbf{D}_1 \mathbf{A}. \end{aligned} \quad (\text{A2})$$

Second and third-order derivatives can be computed by defining matrices \mathbf{D}_2 and \mathbf{D}_3 :

$$\begin{aligned} \mathbf{U}_{zz} &= \mathbf{D}_2 \mathbf{A}, \quad D_{ij,2} = [D_{ij,1}]^2, \\ \mathbf{U}_{zzz} &= \mathbf{D}_3 \mathbf{A}, \quad D_{ij,3} = [D_{ij,1}]^3. \end{aligned} \quad (\text{A3})$$

Use of Eqs. (A1)–(A3) allows computation of the modal derivatives using only the values of the modes at fixed points, without having to recourse to numerical differentiation.

APPENDIX B: THE EFFECT OF THE SANR AND SOURCE AMPLITUDE ESTIMATION ON LOCALIZATION PERFORMANCE

It is demonstrated here that the addition of the modulus of source amplitude $\alpha = |A(\omega)|$ for the deterministic signal

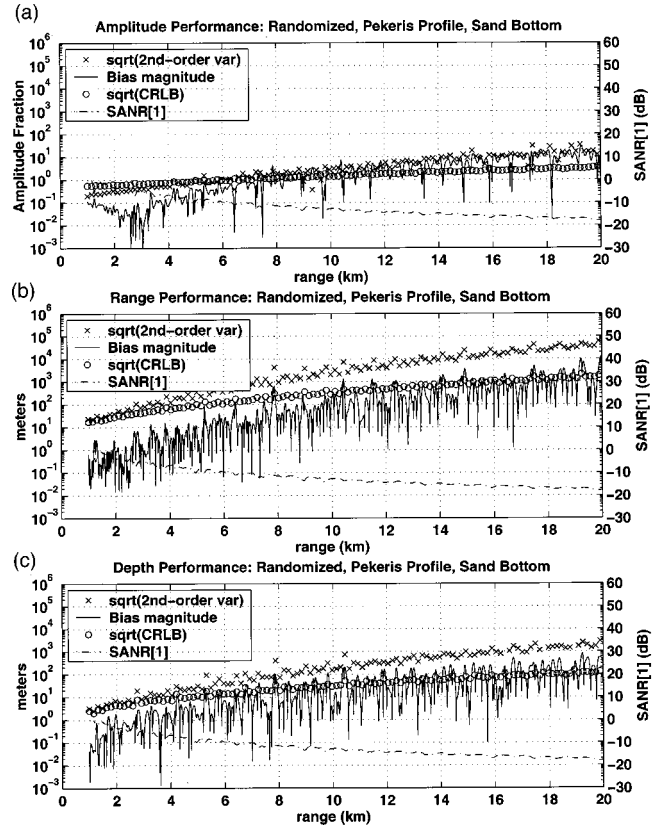


FIG. 25. Random signal single-sample ($n=1$) ocean acoustic MLE performance for (a) amplitude A , (b) range, and (c) depth estimation versus source range, for a 100 Hz signal placed at 50 m depth in the case A environment, a Pekeris waveguide with a sand bottom. The true source amplitude A is 1. A comparison of these results with Fig. 3 shows that the addition of amplitude as an estimation parameter has negligible effect on the MLE localization performance.

model and source power $I_\alpha = \langle |A(\omega)|^2 \rangle$ for the randomized signal model as a third estimation parameter in addition to source range and depth, has only a minor effect on localization performance. The bias and the variance terms are independent of α for the deterministic case and I_α for the randomized case, provided that the SANR[1] remains fixed. Variations between two-parameter and three-parameter-case estimates of range and depth are negligible in our localization scenarios, as we show in the simulations presented in the Figs. 24 and 25. No new derivatives are required to apply Eqs. (2) and (3) to the three-parameter estimation problem, since the source amplitude is linearly related to the data.

We first present analysis for the deterministic scenario and then we discuss the completely randomized case.

1. Deterministic signal model

In the deterministic signal model, according to Eqs. (5a), (5b), and (8), the expected complex vector field can be expressed as a real vector

$$\begin{aligned} \boldsymbol{\mu} &= \alpha \begin{bmatrix} \cos(\phi) \mathbf{I} & -\sin(\phi) \mathbf{I} \\ \sin(\phi) \mathbf{I} & \cos(\phi) \mathbf{I} \end{bmatrix} \begin{bmatrix} \text{Re}(\tilde{\mathbf{g}}(r,z)) \\ \text{Im}(\tilde{\mathbf{g}}(r,z)) \end{bmatrix} \\ &= \alpha \boldsymbol{\Omega} \mathbf{g}(r,z), \end{aligned} \quad (\text{B1})$$

where ϕ is the phase of $A(\omega)$, $\mathbf{\Omega}$ is a rotation matrix of dimension N , \mathbf{I} is the identity matrix of dimension $N/2$ and $\mathbf{g}(r, z)$ is formed with the real part and the imaginary part of $\tilde{\mathbf{g}}(r, z)$. In our complex representation the source phase conveniently scales out of the problem since the matrix $\mathbf{\Omega}$ is orthogonal ($\mathbf{\Omega}^T \mathbf{\Omega} = \mathbf{I}$). It follows that $\boldsymbol{\mu}_r = \alpha \mathbf{\Omega} \mathbf{g}_r(r, z)$, $\boldsymbol{\mu}_z = \alpha \mathbf{\Omega} \mathbf{g}_z(r, z)$, $\boldsymbol{\mu}_\alpha = \mathbf{\Omega} \mathbf{g}(r, z)$, and $\boldsymbol{\mu}_{\alpha\alpha} = 0$, where in this Appendix only the subscripts r , z , and α represent derivatives with respect to range, depth, and source amplitude, respectively. The noise covariance, according to Eqs. (6) and (8) is a diagonal matrix whose trace is given by $\text{tr}(\mathbf{C}^{\text{additive}}) = \sigma^2(N/2)$. From Eqs. (2) and (3), Eqs. (B6)–(B15), and Eqs. (B18)–(B21), we then observe that the first-order bias and the CRLB are proportional to $1/\text{SANR}$, where $\text{SANR} = \text{SANR}[n] = n(2\boldsymbol{\mu}^T \boldsymbol{\mu} / N\sigma^2) = n \text{SANR}[1]$, while the second-order variance is proportional to $1/\text{SANR}^2$. This property explains the dependence of the curves in Figs. 12 and 14 on SANR.

We first consider the problem of estimating two parameters, amplitude and range, to illustrate the issues. We then extend the results to the three-parameter case of amplitude, range, and depth.

From the Appendix of Ref. 12 and the definition above for the mean $\boldsymbol{\mu}$, the Fisher information becomes

$$i = \text{SANR} \frac{N}{2} \begin{bmatrix} \frac{1}{\alpha^2} & \frac{\mathbf{g}_r^T \mathbf{g}_r}{\alpha \mathbf{g}^T \mathbf{g}} \\ \frac{\mathbf{g}_r^T \mathbf{g}_r}{\alpha \mathbf{g}^T \mathbf{g}} & \frac{\mathbf{g}_r^T \mathbf{g}_r}{\mathbf{g}^T \mathbf{g}} \end{bmatrix} \quad (\text{B2})$$

from which the Cramer–Rao bound becomes

$$\text{CRLB} = i^{-1} = \frac{1}{\text{SANR}} \frac{1}{\left(\frac{\mathbf{g}_r^T \mathbf{g}_r}{\mathbf{g}^T \mathbf{g}} - \frac{(\mathbf{g}_r^T \mathbf{g})^2}{\mathbf{g}^T \mathbf{g}} \right) \frac{N}{2}} \times \begin{bmatrix} \overbrace{\alpha^2 \mathbf{g}_r^T \mathbf{g}_r}^{\text{amplitude}} & -\alpha \mathbf{g}^T \mathbf{g}_r \\ -\alpha \mathbf{g}^T \mathbf{g}_r & \underbrace{\mathbf{g}_r^T \mathbf{g}_r}_{\text{range}} \end{bmatrix}. \quad (\text{B3})$$

While the CRLB for the source amplitude scales with α^2 , the CRLB for range is independent of α , for fixed SANR. For range estimation, the square root of the CRLB, which represents a first approximation to the error, becomes

$$\sqrt{\text{CRLB}}(r) = \frac{1}{\sqrt{\frac{N}{2} \text{SANR} \left| \frac{\mathbf{g}_{r,\perp}}{\mathbf{g}} \right|^2}}, \quad (\text{B4})$$

where

$$\left| \frac{\mathbf{g}_{r,\perp}}{\mathbf{g}} \right|^2 = \mathbf{g}_r^T \mathbf{g} \mathbf{g}_r^T \mathbf{g}_r - (\mathbf{g}_r^T \mathbf{g})^2. \quad (\text{B5})$$

As expected, the error decreases for increasing SANR. However, in Eq. (B4) there is also a geometrical interpretation:

the error is not controlled directly by $\mathbf{g}_r^T \mathbf{g}_r$, but by the component of \mathbf{g}_r orthogonal to \mathbf{g} .

A similar analysis is performed for the components of the bias when the tensors

$$v_{\alpha\alpha\alpha} = 0, \quad (\text{B6})$$

$$v_{\alpha\alpha r} = -2n \frac{\mathbf{g}_r^T \mathbf{g}_r}{\sigma^2}, \quad (\text{B7})$$

$$v_{\alpha r r} = -n\alpha \left(\frac{\mathbf{g}_{rr}^T \mathbf{g}}{\sigma^2} + 2 \frac{\mathbf{g}_r^T \mathbf{g}_r}{\sigma^2} \right), \quad (\text{B8})$$

$$v_{r r r} = -3n\alpha^2 \frac{\mathbf{g}_{rr}^T \mathbf{g}_r}{\sigma^2}, \quad (\text{B9})$$

$$v_{\alpha, r r} = n\alpha \frac{\mathbf{g}_{rr}^T \mathbf{g}}{\sigma^2}, \quad (\text{B10})$$

$$v_{\alpha, r \alpha} = n \frac{\mathbf{g}_r^T \mathbf{g}_r}{\sigma^2}, \quad (\text{B11})$$

$$v_{\alpha, \alpha \alpha} = 0, \quad (\text{B12})$$

$$v_{r, \alpha \alpha} = 0, \quad (\text{B13})$$

$$v_{r, r \alpha} = n\alpha \frac{\mathbf{g}_r^T \mathbf{g}_r}{\sigma^2}, \quad (\text{B14})$$

$$v_{r, r r} = n \frac{\mathbf{g}_{rr}^T \mathbf{g}_r}{\sigma^2}, \quad (\text{B15})$$

are substituted in (B2). The first-order bias then becomes

$$\begin{bmatrix} b^\alpha(1) \\ b^r(1) \end{bmatrix} = \frac{1}{\text{SANR} \xi \frac{N}{2}} \left[\begin{bmatrix} \alpha \mathbf{g}_r^T \mathbf{g}_r \\ \mathbf{g}_r^T \mathbf{g}_r \end{bmatrix} \left(\mathbf{g}_{rr}^T \mathbf{g} - 2 \frac{(\mathbf{g}_r^T \mathbf{g})^2}{\mathbf{g}^T \mathbf{g}} \right) + \begin{bmatrix} \alpha \mathbf{g}_r^T \mathbf{g}_r \\ \mathbf{g}_r^T \mathbf{g}_r \end{bmatrix} \left(\mathbf{g}_{rr}^T \mathbf{g}_r - 2 \frac{\mathbf{g}_r^T \mathbf{g} \mathbf{g}_r^T \mathbf{g}_r}{\mathbf{g}^T \mathbf{g}} \right) \right], \quad (\text{B16})$$

where $\xi = \mathbf{g}_r^T \mathbf{g}_r - [(\mathbf{g}_r^T \mathbf{g})^2 / \mathbf{g}^T \mathbf{g}]$. For fixed SANR, the range bias $b^r(1)$ is independent of α while the amplitude bias is proportional to α .

The analysis of the second-order covariance is simpler if we express the terms of order $O_p(n^{-2})$ in Eq. (3) as

we observe that for $\sigma=0$, in the scalar case, where one receiver only is employed, the model remains well defined because the data vector is one dimensional, but $\tilde{\mathbf{C}}^{-1}$ does not exist for $N \geq 2$ because the determinant of $\tilde{\mathbf{C}}$ vanishes.

With the present definition of SANR in the random signal model, terms in Eqs. (2) and (3) of order n^{-m} are generally not of order in SANR^{-m} , in contrast to the situation found for a deterministic signal.

For randomized signals, however, the first order bias, the CRLB, and the second-order variance for range and depth still depend only on the $\text{SANR}[1]$ and not on signal ampli-

tude alone. This can be seen, from the definition of the Fisher information matrix for the randomized case $i_{nm} = \text{tr}(\tilde{\mathbf{C}}^{-1} \tilde{\mathbf{C}}_m \tilde{\mathbf{C}}^{-1} \tilde{\mathbf{C}}_n)$, where $m = \alpha, r$ and $n = \alpha, r$, $\tilde{\mathbf{C}}_\alpha = \partial \tilde{\mathbf{C}} / \partial I_\alpha = \tilde{\mathbf{g}} \tilde{\mathbf{g}}^+$ and $\tilde{\mathbf{C}}_r = \partial \tilde{\mathbf{C}} / \partial r = I_\alpha (\tilde{\mathbf{g}}_r \tilde{\mathbf{g}}_r^+ + \tilde{\mathbf{g}} \tilde{\mathbf{g}}_r^+)$, and

$$\mathbf{C}^{-1} = \frac{1}{\sigma^2} \begin{bmatrix} I_\alpha \tilde{\mathbf{g}} \tilde{\mathbf{g}}^+ \\ I_\alpha \tilde{\mathbf{g}}_r \tilde{\mathbf{g}}_r^+ + \tilde{\mathbf{g}} \tilde{\mathbf{g}}_r^+ \\ 1 + \frac{I_\alpha}{\sigma^2} |\tilde{\mathbf{g}}|^2 \end{bmatrix}. \quad (\text{B28})$$

The Fisher information matrix becomes

$$i = n \left(\frac{\frac{N}{2} \text{SANR}[1]}{1 + \frac{N}{2} \text{SANR}[1]} \right)^2 \begin{bmatrix} \frac{1}{I_\alpha^2} & \frac{1}{I_\alpha} \frac{(\tilde{\mathbf{g}}_r^+ \tilde{\mathbf{g}} + \tilde{\mathbf{g}}^+ \tilde{\mathbf{g}}_r)}{|\tilde{\mathbf{g}}|^2} \\ \frac{1}{I_\alpha} \frac{(\tilde{\mathbf{g}}_r^+ \tilde{\mathbf{g}} + \tilde{\mathbf{g}}^+ \tilde{\mathbf{g}}_r)}{|\tilde{\mathbf{g}}|^2} & \frac{1}{|\tilde{\mathbf{g}}|^4} \left((\tilde{\mathbf{g}}^+ \tilde{\mathbf{g}} + \tilde{\mathbf{g}}^+ \tilde{\mathbf{g}})^2 + 2 \left(1 + \frac{N}{2} \text{SANR}[1] \right) (|\tilde{\mathbf{g}}_r|^2 |\tilde{\mathbf{g}}|^2 - \tilde{\mathbf{g}}_r^+ \tilde{\mathbf{g}} \tilde{\mathbf{g}}_r^+) \right) \end{bmatrix} \quad (\text{B29})$$

with CRLB,

$$\text{CRLB} = \frac{\Delta}{n \left(\frac{N}{2} \text{SANR}[1] \right)^2} \begin{bmatrix} I_\alpha^2 \frac{1}{|\tilde{\mathbf{g}}|^4} \left((\tilde{\mathbf{g}}^+ \tilde{\mathbf{g}} + \tilde{\mathbf{g}}^+ \tilde{\mathbf{g}})^2 + 2 \left(1 + \frac{N}{2} \text{SANR}[1] \right) (|\tilde{\mathbf{g}}_r|^2 |\tilde{\mathbf{g}}|^2 - \tilde{\mathbf{g}}_r^+ \tilde{\mathbf{g}} \tilde{\mathbf{g}}_r^+) \right) & -2I_\alpha \frac{\tilde{\mathbf{g}}_r^+ \tilde{\mathbf{g}} + \tilde{\mathbf{g}}^+ \tilde{\mathbf{g}}_r}{|\tilde{\mathbf{g}}|^2} \\ -2I_\alpha \frac{\tilde{\mathbf{g}}_r^+ \tilde{\mathbf{g}} + \tilde{\mathbf{g}}^+ \tilde{\mathbf{g}}_r}{|\tilde{\mathbf{g}}|^2} & 1 \end{bmatrix}, \quad (\text{B30})$$

where

$$\Delta = \frac{1}{2} \left(1 + \frac{N}{2} \text{SANR}[1] \right) \left| \frac{\tilde{\mathbf{g}}_{r,\perp}}{\tilde{\mathbf{g}}} \right|^{-2}.$$

This explicitly shows that the range CRLB is independent of I_α , while the intensity CRLB scales as I_α^2 for fixed $\text{SANR}[1]$.

As in the deterministic signal model, the moments of the asymptotic expansion can be expressed as a product of a function depending on $\text{SANR}[1]$ and a function depending on the geometric properties of the received signal vector. For instance from Eq. (B30) we find that

$$\text{CRLB}(r) = \frac{1}{2n} \frac{1 + \frac{N}{2} \text{SANR}[1]}{\left(\frac{N}{2} \text{SANR}[1] \left| \frac{\tilde{\mathbf{g}}_{r,\perp}}{\tilde{\mathbf{g}}} \right| \right)^2}. \quad (\text{B31})$$

Equation (B31) is only valid for $N/2 > 1$, and $\text{SANR}[1]$ not equal to infinity, so that it does not apply to scalar parameter estimates from scalar data.

After similar analysis, too detailed to present for the full three-parameter randomized signal case, we find that the first order bias, the CRLB, and the second-order variance for range and depth depend only on the $\text{SANR}[1]$ and not on I_α alone as expected.

¹O. Diachok, A. Caiti, P. Gerstoft, and H. Schmidt, *Full Field Inversion Methods in Ocean and Seismic Acoustics* (Kluwer, Dordrecht, 1995).

²A. B. Baggeroer, W. A. Kuperman, and P. N. Mikhalevsky, "An overview of matched field methods in ocean acoustics," *IEEE J. Ocean. Eng.* **18**, 401–424 (1993).

³F. B. Jensen, W. A. Kuperman, M. B. Porter, and H. Schmidt, *Computational Ocean Acoustics* (American Institute of Physics, New York, 1994).

⁴C. R. Rao, *Linear Statistical Inference and its Applications* (Wiley, New York, 1973).

⁵A. B. Baggeroer, W. A. Kuperman, and H. Schmidt, "Matched field processing: source localization in correlated noise as an optimum parameter estimation problem," *J. Acoust. Soc. Am.* **83**, 571–587 (1988).

⁶M. J. Hinich and E. J. Sullivan, "Maximum-likelihood passive localization using mode filtering," *J. Acoust. Soc. Am.* **85**, 214–219 (1989).

⁷A. J. Weiss and E. Weinstein, "Fundamental limitations in passive time delay estimation," *IEEE Trans. Acoust., Speech, Signal Process.* **ASSP-31**, 472–485 (1983).

⁸A. J. Weiss and E. Weinstein, Lower bounds in parameter estimation—summary of results, presented at ICASSP, Tokyo, 1986.

⁹D. Chazan, M. Zakai, and J. Ziv, "Improved lower bounds on signal parameter estimation," *IEEE Trans. Inf. Theory* **IT-21**, 90–93 (1975).

¹⁰E. W. Barankin, "Locally best unbiased estimates," *Ann. Math. Stat.* **20**, 477–501 (1949).

¹¹J. Tabrikian, "Barankin Bounds for Source Localization in an Uncertain Ocean Environment," *IEEE Trans. Signal Process.* **47**, 2917–2927 (1999).

¹²E. Naftali and N. C. Makris, "Necessary conditions for a maximum-likelihood estimate to become asymptotically unbiased and attain the Cramer-Rao lower bound. I. General approach with an application to time-delay and doppler shift estimation," *J. Acoust. Soc. Am.* **110**, 1917–1930 (2001). [Errata: in Sec. IV the order of the polynomials in all equations should have SNR replace sample size n , since $n=1$ in Eq. (12). Also in Eq. (23) the factor $8\omega_c^2$ should be replaced with $6\omega_c^2$ and the factor $3\omega_c^4$ should be replaced with ω_c^4 .]

¹³R. L. Parker, *Geophysical Inverse Theory* (Princeton University Press, Princeton, New Jersey, 1994).

¹⁴S. M. Kay, *Fundamentals of Statistical Signal Processing: Estimation Theory* (Prentice-Hall, Englewood Cliffs, NJ, 1993), Vol. 1.

- ¹⁵E. J. Sullivan and D. Middleton, "Estimation and detection issues in matched-field processing," *IEEE J. Ocean. Eng.* **18**, 156–167 (1993).
- ¹⁶H. P. Bucker, "Use of calculated sound fields and matched field detection to locate sound sources in shallow water," *J. Acoust. Soc. Am.* **59**, 368–373 (1976).
- ¹⁷O. E. Barndorff-Nielsen and D. R. Cox, *Inference and Asymptotics* (Chapman and Hall, London, 1994).
- ¹⁸L. L. Van Trees, *Detection, Estimation and Modulation Theory* (Wiley, New York, 1970), Vol. III.
- ¹⁹N. C. Makris, "Parameter resolution bounds that depend on sample size," *J. Acoust. Soc. Am.* **99**, 2851–2861 (1996). The misstatement in this paper that the distribution for the sample covariance of a CCGR data vector is unknown is corrected in Ref. 20 below. The distribution in question is the complex Wishart distribution.
- ²⁰N. C. Makris, "The statistics of ocean-acoustic ambient noise," in *Sea Surface Sound*, edited by T. Leighton (Kluwer Academic, Dordrecht, 1997).
- ²¹J. H. Goodman, *Statistical Optics* (Wiley-Interscience, New York, 1985).
- ²²N. C. Makris, "The effect of saturated transmission scintillation on ocean acoustic intensity measurements," *J. Acoust. Soc. Am.* **100**, 769–783 (1996).
- ²³N. Levanon, *Radar Principles* (Wiley, New York, 1988).
- ²⁴P. Swerling, "Probability of detection for fluctuating targets," *Trans. IRE Prof. Group Inf. Theory* **IT-6**, 269–308 (1960).
- ²⁵P. G. Bergmann, "Intensity fluctuations," in *The Physics of Sound in the Sea, Part I: Transmission* (National Defense Research Committee, Washington, DC, 1946).
- ²⁶J. L. Krolik, "Matched-field minimum variance beamforming in a random ocean channel," *J. Acoust. Soc. Am.* **92**, 1408–1419 (1992).
- ²⁷J. Krolik and G. Niezgoda, "Wideband matched-field processing in a random ocean channel," presented at Acoustic Signal Processing for Ocean Exploration, 1993.
- ²⁸N. O. Booth, P. A. Baxley, J. A. Rice, P. W. Schey, W. S. Hodgkiss, G. L. D'Spain, and J. J. Murray, "Source localization with broad-band matched-field processing in shallow water," *IEEE J. Ocean. Eng.* **21**, 402–412 (1996).
- ²⁹J. Rice and J. Determan, "SWellEx-3 Data Report," NCCOSC RDT&E Division, Code 541, Tech Rept. 1995.
- ³⁰W. A. Kuperman and F. Ingenito, "Spatial correlation of surface generated noise in a stratified ocean," *J. Acoust. Soc. Am.* **67**, 1988–1996 (1980).
- ³¹P. M. Morse and H. Feshbach, *Methods of Theoretical Physics* (McGraw-Hill, New York, 1953), Vol. II.